UNIVERSITY TRANSPORTATION CENTER
FOR UNDERGROUND TRANSPORTATION INFRASTRUCTURE

DETERMINISTIC AND PROBABILISTIC ANALYSIS OF THE EFFECT OF TUNNEL LOCATION ON SLOPE STABILITY - APPLICATION TO THE EISENHOWER-JOHNSON MEMORIAL TUNNEL

FINAL PROJECT REPORT

by
Simon Baeza-Faundez
Marte Gutierrez

University Transportation Center for
Underground Transportation Infrastructure
(UTC-UTI)
Colorado School of Mines

Sponsorship

US Department Transportation
Contract/Grant No. 69A355174711

October 31, 2022

COLORADO SCHOOL OF MINES
EARTH • ENERGY • ENVIRONMENT

Disclaimer

The contents of this report reflect the views of the authors, who are responsible for the facts and the accuracy of the information presented herein. This document is disseminated in the interest of information exchange. The report is funded, partially or entirely, by grants from U.S. Department of Transportation's University Transportation Centers Program. However, the U.S. Government assumes no liability for the contents or use thereof.

1. Report No. 11	2. Government Accession No.	3. Recipient's Catalog No.	
4. Title and Subtitle Deterministic and probabilistic analysis of the effect of tunnel location on slope stability - application to the Eisenhower-Johnson Memorial Tunnel		5. Report Date October 2022	
		6. Performing Organization Code	
7. Author(s) Marte Gutierrez (Orcid.org/0000-0001-5070-8726) Simon Baeza-Faundez		8. Performing Organization Report No.	
9. Performing Organization Name and Address University Transportation Center for Underground Transportation Infrastructure (UTC-UTI) Tier 1 University Transportation Center Colorado School of Mines Coolbaugh 308, 1012 14th St., Golden, CO 80401		10. Work Unit No. (TRAIS)	
		11. Contract or Grant No.	
12. Sponsoring Agency Name and Address United States of America Department of Transportation Research and Innovative Technology Administration		13. Type of Report and Period Covered	
		14. Sponsoring Agency Code	
15. Supplementary Notes Report also available at: https://zenodo.org/communities/utc-uti			
16. Abstract Subsurface characterization in mountainous terrain is complex, requiring extensive analysis to optimize tunnel alignment based on rock quality, support systems, and groundwater flow. However, slope stability is often underexamined, especially for tunnels aligned parallel to slope faces. This is due to the rapidly changing terrain geometry, which increases the cost of detailed 3D modeling, leading to reliance on 2D simulations. This study uses the Eisenhower-Johnson Memorial Tunnel (EJMT) in Colorado to determine the minimum distance from the slope face at which slope stability is unaffected. Results from 600 simulations show stability improves as tunnels move deeper, with interaction minimized beyond 5.5 tunnel diameters. The study also includes access road considerations and a 3D analysis for perpendicular alignments.			
17. Key Words: Tunneling, slope stability, landslide, deterministic, probabilistic, factor of safety		18. Distribution Statement No restrictions.	
19. Security Classification (of this report) Unclassified	20. Security Classification (of this page) Unclassified	21. No of Pages 93	22. Price NA

EXECUTIVE SUMMARY

The inherent complexity of subsurface characterization in mountainous terrains typically results in extensive analyses to optimize tunnel alignments based on parameters such as rock quality, support systems, and groundwater flow. However, limited investigations are performed to determine the influence of slope stability on the selection of tunnel location for alignments relatively parallel to the slope face. One of the major limitations of these investigations relies on the rapidly changing geometry of mountainous environments, which significantly increases the computational cost required to model detailed three-dimensional slopes. As such, slope stability analyses are often idealized using two-dimensional simulations. In this research, a case study of the Eisenhower-Johnson Memorial Tunnel (EJMT) in Colorado is incorporated to determine the minimum distance between a dual-bore tunnel and the face of the slope at which slope stability is virtually unaltered, using two-dimensional numerical simulations. The results from a deterministic and probabilistic analysis of approximately 600 simulations suggest that slope stability increases as tunnel bores are translated to areas of increasing overburden. Specifically, tunnel-slope interaction was minimized past a horizontal distance of 5.5 times the diameter of the tunnels into the slope. Complementary analyses associated with the EJMT tunnel construction, including access roads and a three-dimensional analysis of a tunnel alignment relatively perpendicular to the slope face, are included in this document. The author believes this research provides a general trend that could be applied to other projects with geomechanical properties and slope geometry within the ranges used in this study.

TABLE OF CONTENTS

LIST OF FIGURES

LIST OF TABLES

LIST OF SYMBOLS

S	shear strength
c	cohesion in terms of total stress
c’	cohesion in terms of effective stress
σ	total normal stress
u	pore pressure
ϕ	friction angle in terms of total stress
ϕ’	friction angle in terms of effective stress
τ	shear stress
F	factor of safety
τ_m	mobilized shear strength
c_m	mobilized cohesion
ϕ_m	mobilized friction angle
γ	bulk unit weight
γ_{sat}	saturated unit weight
ε	strain
W	weight of the soil mass above the slip surface
Δl	length of a slice
CDOLA	Colorado Department of Local Affairs
CDOT	Colorado Department of Transportation
CDH	Colorado Department of Highways
EJMT	Eisenhower-Johnson Memorial Tunnels
USBR	U.S. Bureau of Reclamation
USGS	U.S. Geological Service

ACKNOWLEDGMENTS

This work was supported by the U.S. Department of Transportation (DOT) under Grant Number: 69A3551747118. The opinions expressed in this report are those of the authors and not the DOT.

CHAPTER 1:
INTRODUCTION

In the last decade, the population in Colorado has increased approximately 14.5%, at an average rate of 0.8% per year. It is one of the states with the more significant percentage of population increase in the United States, and according to projections, this trend will continue for the following decades (CDOTb, 2010). As a result of the population growth, traffic has also increased, particularly between the Denver metropolitan area and nearby cities. For instance, the average daily traffic through the Eisenhower Johnson Memorial Tunnels (EJMT) has more than quadrupled since the opening of the first tunnel and is expected to continue to rise, as shown in Figure 1.1.

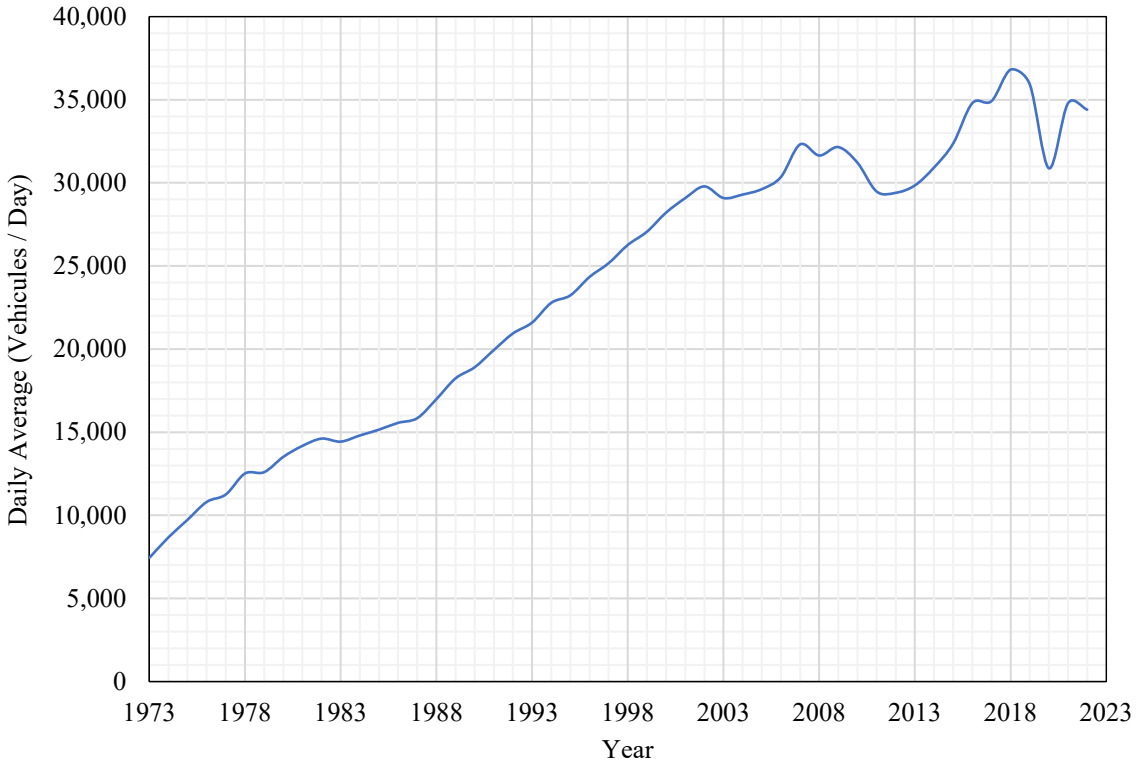

Figure 1.1: Colorado's population forecast from 2000 to 2050 (CDOT, n.d.).

The current traffic volume on Interstate 70 (I-70) Mountain Corridor far exceeds any estimates that could be imagined during its planning and design in the 1960s. The frequent heavy traffic and substantial delays harm the state's economy, decrease mobility, compromise emergency service providers' response, and increase accidents. Hence, continuous efforts to improve transportation in the area have taken place, including this research.

The high elevation, limited space for highway expansion, geological hazards inherent to mountainous terrain, environmental sensitivity, and community values were some challenges considered to suggest transportation improvements for the I-70 Mountain Corridor. The alternatives proposed include transportation management, localized highway improvements, and construction of alternate routes and tunnels, particularly the construction of additional bores at both the Eisenhower-Johnson Memorial Tunnels and the Twin Tunnels and three new high-speed tunnels (65 mph) at the Down Canyon and Floyd Hill areas (CDOTb, 2010).

The construction of additional tunnel bores at the EJMT carries several extra challenges. For example, the construction of the east plaza in the 1960s triggered a landslide of significant proportions, which was stabilized a decade later. Therefore, it is crucial to determine if the slopes nearby the existing tunnels are sufficiently stable for constructing the new tunnel bores. In order to accomplish this goal, general and specific objectives have been considered:

1.1 General Objectives

The primary purpose of this research is to determine the optimal location of the new Eisenhower-Johnson Tunnels considering slope stability as a critical parameter.

1.2 Specific Objectives

This study placed particular emphasis on the following items:

- Determine the geological setting and analyze the effect of geological features on slope stability.
- Validate outdated slope stability studies using current methodologies and available software.
- Perform sensitivity analysis to assess the uncertainty of critical parameters like slope geometry, material properties, depth to the groundwater table, and external loads.
- Determine the inherent probability of failure of the slopes in the vicinity of the Eisenhower Johnson Memorial Tunnels and assess its sensitivity to the parameters mentioned above.
- Determine the optimum tunnel location based on slope stability.

CHAPTER 2:
SITE CHARACTERIZATION

2.1 Site Location

The location of the research site is in the Rocky Mountains along I-70, about 60 miles west of Denver, Colorado. Specifically, the area in the vicinity of the EJMT shown in Figure 2.1.

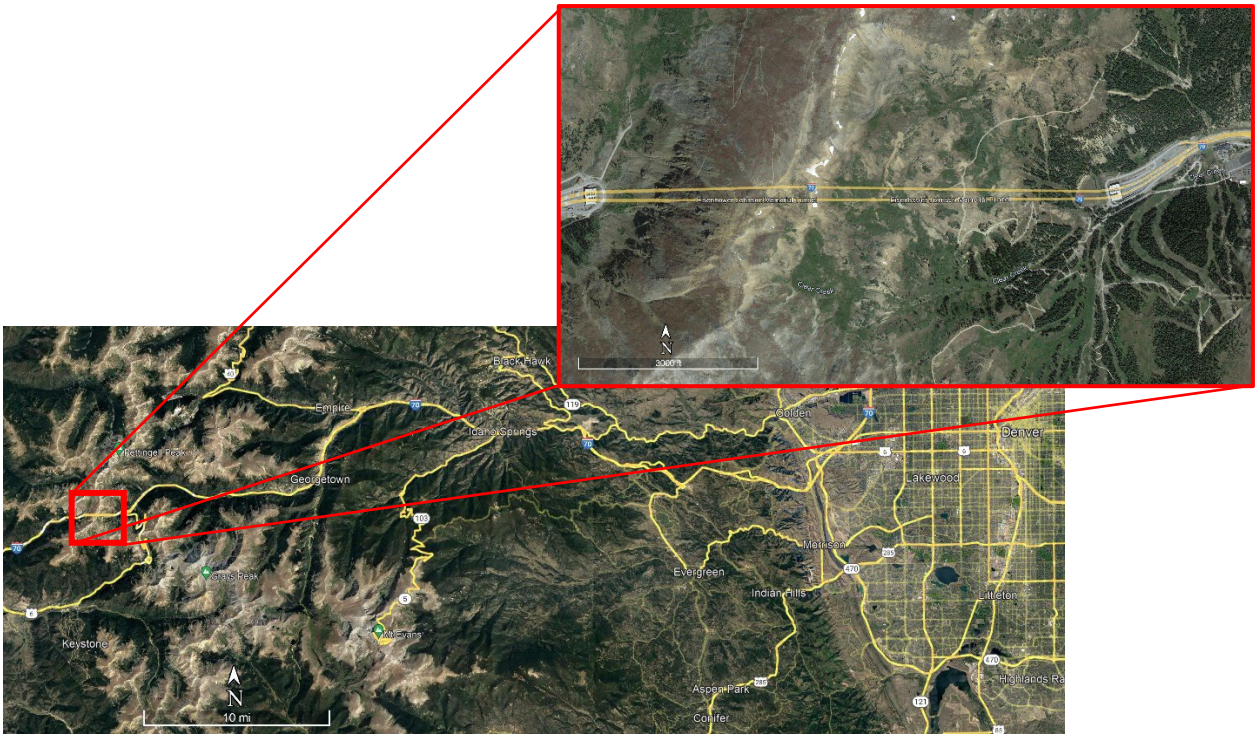

Figure 2.1: Aerial view highlighting the location of interest (Map data: ©2022 Google)

2.2 Eisenhower-Johnson Memorial Tunnel

The EJMT is a dual-bore, four-lane vehicular tunnel located in mountainous terrain at approximately 11,110 ft elevation. It carries I-70 connecting Summit County and Clear Creek County on the eastern and western sides of the Continental Divide. The tunnels are approximately 1.7 miles long, 50 ft high, and 40 ft wide. The alignment of the Pilot/Johnson bore is relatively straight, whereas the Eisenhower bore trends slightly north, reaching a maximum point of separation of about 230 ft at approximately midway. Both bores are about 120 ft apart at the portals. The overburden depth at the maximum elevation point is approximately 1500 ft. Drill-and-Blast was the preferred excavation method, and a horseshoe section with and without an invert strut can be found along the alignment. The changes in

shape were probably related to the variable stress conditions, rock type, and unexpected rock mass behavior encountered during excavation, as described in the following chapters.

2.3 Loveland Basin Landslide

The Loveland Basin Landslide occurred in the spring of 1963 during the excavation of an access road to construct the east portal (Robinson, et al., 1972). Geological and geophysical investigations determined the slide had a volume of approximately 1,700,000 cubic yards of dimensions of 1.500 ft long, 800 ft wide, and a maximum thickness of 70 ft (Robinson, et al., 1974). Early stabilization attempts consisted of constructing a 47,217 cubic-yard buttress, drainage, and the relocation of the Eisenhower bore approximately 150 ft south and 16 ft lower than initially planned. After a decade of research and remediation measures, a buttress equaling approximately 20% of the slide mass stabilized the landslide (Robinson, et al., 1972).

Several slope stability analyses of the landslide were performed from 1963 until 1971, summarized in Table 2.1. The deformations at the Loveland Basin landslide were significant and intricate, often becoming progressively deeper, which was not achievable by a sudden failure mechanism (Lee & Mystkowski, 1979). Furthermore, it was believed that the movement of the slide would be slow, and landslide material would be deposited onto the surface of the initial buttress forming a natural-additional buttress. Therefore, the natural expansion of the buttress, in addition to the reduction of the driving forces due to the loss of material on the slide, would create enough resistance to prevent the landslide from reaching the east plaza (Lee & Mystkowski, 1979). This assumption was critical during the remediation and stabilization process because of the lack of material to construct a bigger buttress. Although the analysts were correct in terms of the speed of failure, stabilization was not complete until the buttress reached the volume recommended by TAMS, as shown in Figure 2.2.

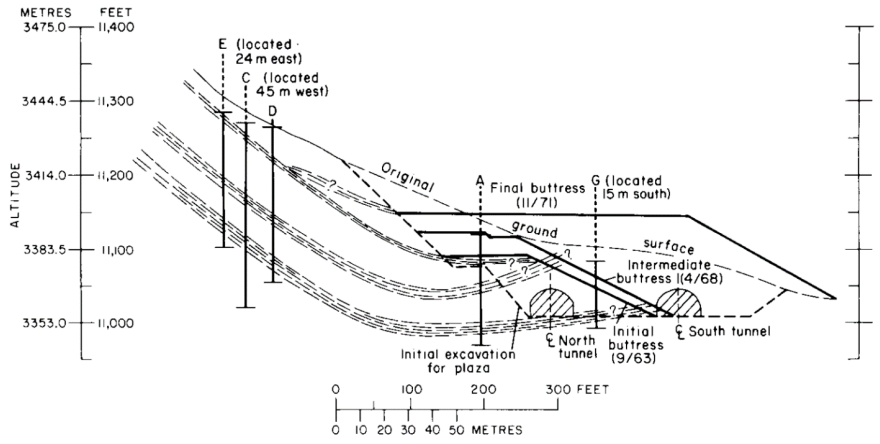

Figure 2.2: Cross-section of the EJMT east portal and the Loveland Basin landslide showing the progressive enlargement of the buttress (Lee & Mystkowski, 1979).

Table 2.1: Summary of slope stability analysis results of the Loveland Basin Landslide, the considerations and geomechanical properties used by the analysts, and their recommendations based on Lee & Mystkowski (1979).

Analysts	Year	Method, Considerations, and Geomechanical Properties	F	Recommendations
R.A. Bohman (FHWA)	1963	Used preliminary electric resistivity data, measured dimensions, and assumed physical properties. The method was not specified.	1.40* 1.00	Construction of a buttress of 76,000 m^3 (100,000 yd^3) of compacted material. However, only a 47,220-m^3 buttress (61,700 yd^3) was constructed[1].
R.A. Bohman[2] (Robinson, et al., 1972)	1964	Used the Baker and Yoder method. No water table data was available then, so it was not considered.	1.00	Shift the position of the Pilot Bore to the south (away from the slide), lower the pilot bore and approach grade, and move the east portal to the east.
TAMS	1966	Reviewed previous data and used inclinometers. Considered a $\phi = 34$, the water level at the surface, and a saturated unit weight of 2.4 Mg/m^3.	1.80	Construction of an additional buttress of 279,000 m^3 to an altitude of 11,150 ft to achieve a 326,000-m^3 final buttress (426,000 yd^3)
D.U. Deere and F.D. Patton (Contractor)	N/F	Used two methods: 1) Infinite Slope ($\phi = 34$ and water level at 6 m at the toe of the slide) 2) Sliding Wedge ($\phi = 31$)	1.06[3] 1.56*	Construction of a total buttress of 306,000 m^3 (400,000 yd^3). Also, draining the slide's toe would increase the value of F by 0.1.
Colorado Division of Highways	1971	Used Morgenstern and Price method. Considered to types of material properties: Landslide ($\phi = 34$, $c = 0$, and unit weight = 2.5 Mg/m^3) and Buttress ($\phi=30$, $c=$ 68.9 kN/m^2, and unit weight = 2.4 Mg/m^3). Water level not specified.	1.75[4] 2.81[5]	The final buttress recommended by TAMS showed to stabilize the slope successfully. No further recommendations.

* Estimation for the factor of safety for the given recommendations and not the actual result for the conditions at the moment of the analysis.
[1] The first buttress constructed did not met the recommendation issued by Bohman mainly due to lack of material.
[2] A detailed description of this slope stability analysis is presented in Robinson et al. (1972).
[3] Not information found about the actual conditions at the moment of the analysis, but it is suggested that was an intermediate point between the initial buttress of 61,700 yd^3 and the final buttress suggested by TAMS.
[4] For deep movement, i.e., approximately from 141 to 164 ft deep.
[5] For shallow movement, i.e., approximately from 98 to 125 ft deep.

Studies regarding the Loveland Basin landslide have not been recently published, nor records of detectable movement were found on governmental platforms such as the Colorado Department of Transportation (CDOT). However, a comparison of old and newer trees in the area showed that movement has occurred in the past, as shown in Figure 2.3-A. Generally, curved trunks suggest a slope moved faster downslope than the growth rate of the tree (Harker, 1996). Furthermore, the trunks curvature typically describes two types of shape: d-shape and i-shape. The former could result from creep movement or dormant landslides. On the other hand, i-shaped trunks could result from snow loads or fast landslides. Figure 2.3-B shows that younger trees on the Loveland Basin Landslide have little to no curvature in their trunks, suggesting that recent movement is inexistent or negligible.

Figure 2.3: Images of typical tree trunks on the Loveland Basin landslide showing: A) older, d-shaped tree trunks and B) younger, straight, unaltered tree trunks.

2.4 Site Geology

The geology on both sides of the Continental Divide is relatively different. Granite from the Precambrian period is found on the western side, whereas the east side consists of granites and

granite/migmatite[6] mixtures that are less stable (CDOTa, 2010) Robinson, et al. (1974)[7] mapped the rock mass along the EJMT alignment as 75.4% of granite, 23.8% of metasedimentary rocks, and 0.8% of dikes. In many studies, the granite materials in the area have been simplified as Silver Plume Granite (SPG) with inclusions of metamorphic rocks of the Idaho Springs Formation (ISF) (Robinson & Lee, 1965; Richards, 1963; Alexander, 2022).

According to Alexander (2022), extensive shearing, faulting, and a higher level of inclusions of the ISF were mapped from the east portal to about 1000 ft west, whereas the western side showed consistent foliation orientations in the SPG, minimal inclusions of the ISF, and intermittent faults.

The U-shaped valleys at the Straight Creek and the Clear Creek and the ground moraine deposits at the east and west valleys of the EJMT suggest that the area was shaped mainly by glaciation. A section of the geologic map of the Montezuma Quadrangle in Colorado is shown in Figure 2.4.

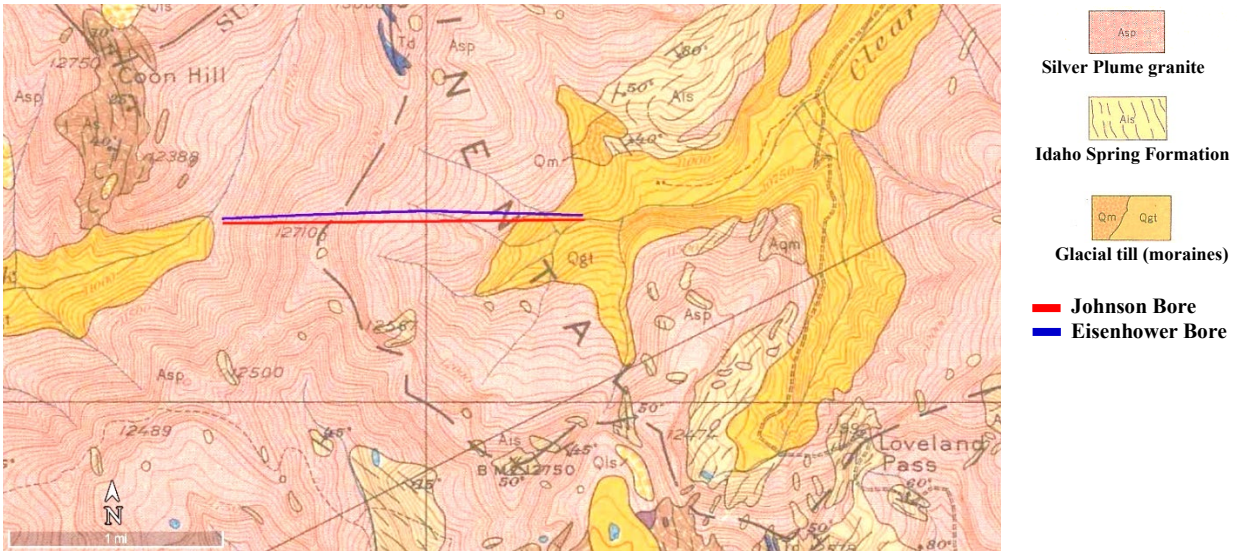

Figure 2.4: Section of the geologic map of Montezuma Quadrangle, Colorado, showing the EJMT alignment (USGS, 1935)[8]

2.4.1 Igneous Rocks

According to Robinson et al. (1974), the granite in the research area was a medium-grained, slightly porphyritic biotite granite with approximately equal amounts of microcline (potassium feldspar),

[6] Migmatites is a heterogeneous metamorphic rock formed by anatexis, i.e., partial melting.

[7] The results from surficial mapping was performed several years before and published in several papers (also mentioned in this study). However, the most recent publication was used.

[8] Sized reduced from original for space purposes.

plagioclase feldspar, and quartz; which resembled the composition of the SPG. The plagioclase grains were partially altered to sericite and clay minerals. The quartz generally occurred as aggregates to the feldspar grains or as small distinct grains in the microcline. Partially altered biotite and muscovite were found in minor quantities. Zircon, monazite, apatite (accessory minerals), and magnetite and pyrite (opaque minerals) appeared as inclusions in the biotite. Furthermore, the alteration of granitic materials was directly related to the degree of fracturing, i.e., alteration typically occurred along joints, faults, and within shear zones (Robinson & Lee, 1965; Richards, 1963). For simplicity, this research assumed all granitic materials to be SPG.

2.4.2 Metamorphic Rocks

The metamorphic rocks found in the area were presumably of sedimentary origin (Robinson, et al., 1974). This metasedimentary material, primarily located at the east side of the continental divide, consisted of a wide range of biotite-quartz-plagioclase gneisses with a significant amount of microcline and muscovite. Hornblende and sillimanite were locally common, and accessory and opaque minerals were also present. Most plagioclase had been altered to clay minerals and sericite alongside cleavage fractures. Fractures were filled with quartz and microcline due to cataclastic effects, and biotite had been partially or entirely altered to chlorite. Usually, fresh microcline was present more extensively nearby layers of granite. Generally, the gneisses were interbanded with granitic material, i.e., found as inclusions in the granite (Robinson & Lee, 1965). In the present study, the metasedimentary rocks were assumed to be ISF.

2.4.3 Dikes

A series of augite diorite dikes (intrusive rocks) were found in the vicinity of the continental divide during the surficial recognizance and construction of the EJMT. For instance, the closest dike outcrop was mapped about 1000 feet north of the tunnel line, and at the tunnel level, the dikes arose approximately a mile west of the east portal (Robinson, et al., 1974; Mattei, 1965). The dikes' dimensions ranged from a few feet to more than 1,000 ft in length and from less than a foot to 200 ft in width.

Dikes were steeply dipping, northerly trending, cross-cutting the bedrock foliation, and noticeably magnetic (Richards, 1963). Petrographic examination of a sample taken by Richards indicated that these rocks could be described as an altered magnetite-bearing gabbro (50-55% calcic plagioclase, 35-40% of augite, and 10-12% of magnetite). The geologic analysis performed by Robinson et al. (1974) closely agreed with those results obtained by Richards (1963), stating that the augite diorite dikes consist of similar percentages of plagioclase feldspar and ferromagnesian minerals.

Furthermore, the outcrops in the vicinity of these dikes were only gently fractured and rarely altered (Robinson, et al., 1974; Richards, 1963), forming a relatively competent rock requiring minimal to no support during tunnel construction (Mattei, 1965).

2.4.4 Fault Gouge Material

Strictly geologically speaking, fault gouge is a "crushed and ground-up rock produced by friction between the two sides when a fault moves" (USGS, n.d.). Along the EJMT, this material resulted from extensive mechanical grinding and chemical alteration of the grains of SPG and ISF adjacent to faults and shear zones. The primary alteration agent of these ground materials was groundwater, which primarily produced clay minerals, chlorite, and silica (Robinson, et al., 1974).

2.4.5 Surficial Deposits

The primary surficial deposits mapped in the vicinity of the EJMT were till (morainal material), swamp, and alluvial deposits at lower elevations and colluvial deposits of silty and sandy soil, talus, and landslides on the upper slopes (Robinson & Lee, 1965).

Lee and Mystkowski (1979) stated that the morainal material consisted of a well-compacted mixture of clay, sand, gravel, and boulders. Furthermore, Robinson & Hazlewood (1962)[9] determined by seismic investigations that the deposits of morainal material near the east portal before the pilot bore's construction ranged from 0 to 50 ft. in depth. Swamp deposits were removed during the construction of I-70 and the EJMT's east portal (Robinson, et al., 1974).

Typically, talus and boulders accumulate at the base of cliffs such as those found on the west face of the continental divide. According to Lee & Mystowski (1979), boulder deposits ranged from 1 to 16 ft. in thickness, and colluvial deposits of sandy and silty soil had a thickness of up to 3 ft. Landslide material was found northwest of the east portal on the Loveland Basin Landslide (see section 2.3).

2.5 Geomechanical Properties

Alexander (2022) determined the geomechanical properties of typical materials found in the vicinity of the EJMT using historical in-situ and laboratory test data collected by the U.S. Bureau of Reclamation (USBR) and the U.S. Geological Service (USGS) and performing laboratory testing. The ISF sample set varied from schistose to more gneissic material, including several migmatite samples (gneissic end of the sample set). From 24 samples, 30% failed along the foliation and 70% across the foliation. Furthermore, the non-foliation failure mode samples did not show a clear trend between strength

[9] This is an unpublished study and therefore it will not be included in the references. However, this information was obtained from Robinson et al. (1974).

and foliation orientation, suggesting that the ISF material behaves in a relatively isotropic manner. The data used to construct the Mohr-Coulomb failure envelope was fairly wide scatter, probably related to the large variability of rock types within the ISF material. The strength properties of the SPG were determined using the Hoek-Brown (H-B) failure envelope. The data set showed a relatively good fit for the regression with some scatter data. It is worth noting that the geomechanical properties for the SPG determined by Alexander (2022) correspond to those of the intact material.

The geomechanical properties of the landslide material and buttress fill correspond to those used during early slope stability analysis of the Loveland Basin landside, Specifically, the values used by the CDH in 1971. A summary of the geomechanical properties of all materials found on the site is shown in Table 2.2

Table 2.2: Geomechanical properties of Silver Plume Granite, Idaho Spring Formation rocks, and fault gouge at the research site.

Material	$\boldsymbol{\gamma}$ $\left(\frac{\mathbf{MN}}{\mathbf{m^3}}\right)$	$\boldsymbol{\nu}$	**E (MPa)**	$\emptyset'$ **(deg)**	**c (MPa)**	**UCS (MPa)**	$\mathbf{GSI_P}$	$\mathbf{GSI_R}$	$\mathbf{m_i}$	**D**	**n**
SPG	0.02590	0.3	55,000	-	-	179.6	55	26.3	23	0	0.0105
ISF	0.02600	0.18	25,000	37.5	21.9	-	-	-	-	-	-
Landslide	0.02453	0.3	100	34	0	-	-	-	-	-	0.5
Buttress Fill	0.02354	0.3	300	30	0.0689	-	-	-	-	-	0.5

Note: γ is the unit weight, ν is the poisons ratio, E is Young's modulus, $\emptyset$ is the internal friction angle, c is the cohesion, UCS is the unconfined compressive strength, GSI_P is peak geological strength index, GSI_R is residual geological strength index, m_i is a material constant for the intact rock, D is the disturbance factor, and n is the porosity of the material.

2.6 Site Structure

2.6.1 Foliation

The foliation in the ISF was initially parallel to the original sedimentary bedding and locally deformed post-metamorphism. The relative parallelism could have been considered a plane of weakness, but foliation has been extensively contorted (Lovering & Goddard, 1950).

The SPG showed two types of foliations: flow foliation and cataclastic foliation. Flow foliation was found in unfractured and moderately-fractured granite, and it was characterized by parallel

orientation of the semi-porphyritic microcline crystals caused by the movement of the viscous magma during emplacement (Richards, 1963). Similarly, Robinson & Lee (1964) stated that general parallelism of the biotite was seen in biotite-rich granites relative to the potash feldspar, but a random orientation was found for uncontaminated granite. Conversely, cataclastic foliation (less common) was present in granite within or adjacent to shear zones where the micaceous minerals were rotated and streaked out parallel to the shear direction (Robinson, et al., 1974).

2.6.2 Faulting

The EJMT lies within the Loveland Pass fault, which is approximately 2 miles wide, trends about N15°E, and shows a gradational distribution of sheared rock (Robinson & Lee, 1964). The Loveland Pass fault likely originated in the Precambrian period with subsequent faulting during the Tertiary age.

Some samples taken by Robinson & Lee (1964) showed that Precambrian faulting had sheared and stretched the granite grains across shear planes. Furthermore, these planes were healed by either recrystallization or cementing (with microcline or quartz), and the inclusions of metasedimentary rock were stretched parallel to the cataclastic direction in the granite. On the other hand, faults and shear zones from the Tertiary age were characterized by varying degrees of shearing, crushing, and alteration that lacked evidence of recrystallization. The contact zone was typically gradational where the rock had been turned into coarse to fine sand under intense shearing and, when alteration also occurred, to fault gouge, i.e., clay with variable amounts of quartz and feldspar (Miles & Mattei, 1965). The degree of alteration greatly affected the frictional resistance to movement, i.e., the frictional resistance reduced as the alteration of the rocks increased (Richards, 1963).

The striking frequency of most Tertiary faults and shear zones (>5 ft wide) measured at the surface by Robinson & Lee (1964) was N20-50°E, and the second most abundant set strike was N70-80°E. About 4% of faults and shear zones trended parallel to the tunnel alignment, and the major shear zones at angles between 25 to 75° (Figure 2.5). The dip angle for 25% of these faults or shear zones ranged from 35 to 90° and averaged 75°. At the tunnel level, they observed two maximum sets with strike and dip of N45°E, 30° or 70°SE, and N10-20°E, 70-90°SE or 85-90°NW. Similarly, Richards (1963) determined that the probable fold system of the metamorphic rocks appears to trend N26°E, 20°NE, known as the older Precambrian fold system. On the other hand, the more recurrent orientations in the granitic rocks were N17°E, 55°SE, and N17°E, 75°NW (Richards, 1963).

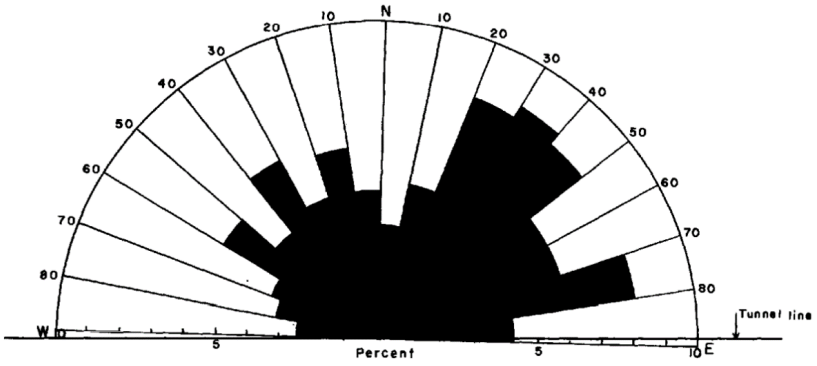

Figure 2.5: Strike frequency of most tertiary faults and shear zones greater than 5 ft wide measured at the surface level (Robinson & Lee, 1964).

Robinson & Lee (1965) mentioned that the width of crushed rock gives the difference between faults and shear zones. Specifically, zones of crushed rock from 5 to 50 ft wide were faults, from 50 to 600 ft wide were shear zones, and less than 5 ft were not considered in the geologic map (too many). However, this is a more theoretical than practical approach.

Some authors have mapped the distribution of fault and shear zones in the vicinity of the EJMT (Richards, 1963; Robinson & Lee, 1965)[10]. These authors agreed that the bedrock on the east side of the continental divide was significantly more faulted and sheared than the bedrock on the west side and that most faults along the tunnel alignment strike NE, as shown in Figure 2.6. However, their interpretations were based on surficial-mapping data, lacking to provide information regarding the vertical orientation of such faults and shear zones. Thus, these models are of limited usefulness for the current research. A most current attempt to develop a geologic model of the fault zone network along the EJMT was reported in Alexander (2022). The author performed a probabilistic extrapolation of surficial mapping to data collected during the construction of the pilot bore reported by Robinson et al. (1974) and Miles & Mattei (1965) and modeled the fault network to depth using Leapfrog Geo, as shown in Figure 2.7.

[10] The original journal article was presented by Robinson & Lee in 1962. However, that version was superseded in 1965 and named *The validity of geologic projection; a successful example: The Straight Creek Tunnel pilot bore, Colorado.* Several papers still cite the original document, but it is no longer available through the USGS and therefore, it will not be mentioned in the references section.

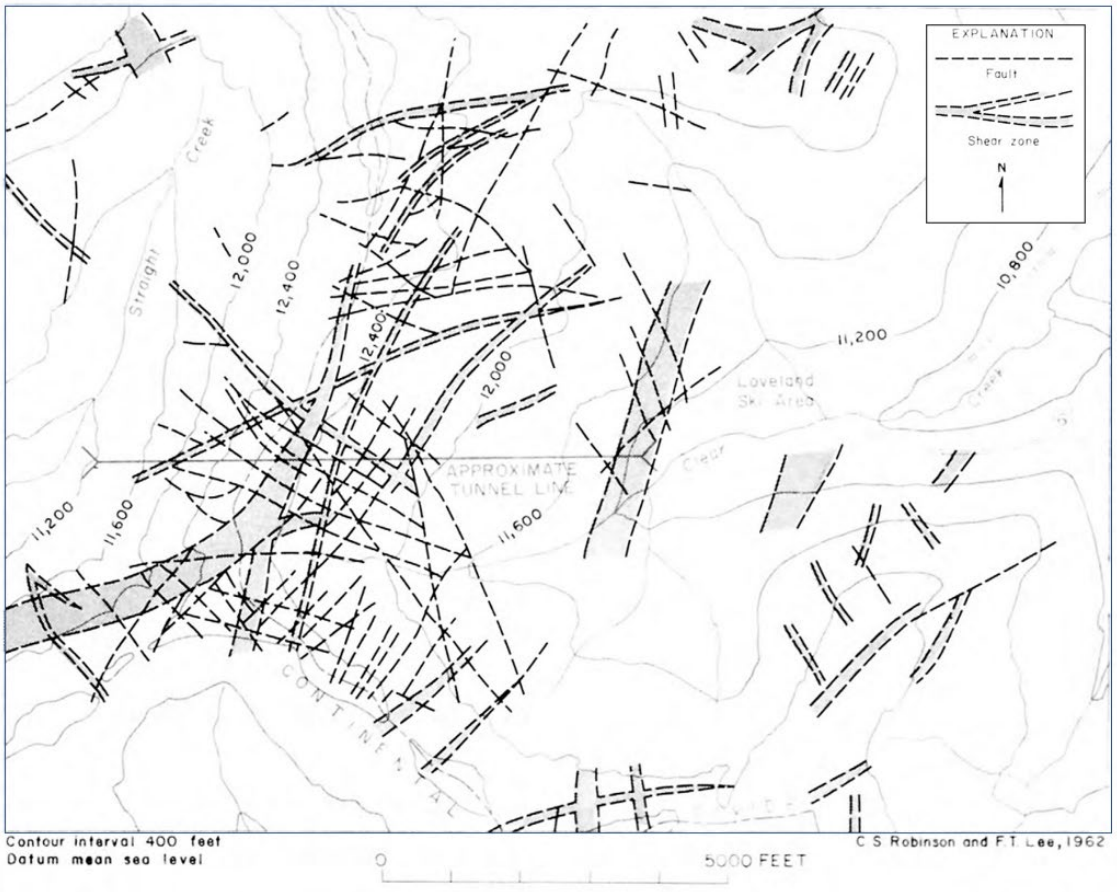

Figure 2.6: Map of the Straight Creek - Clear Creek area showing faults and shear zones greater than 5 ft wide (Robinson & Lee, 1965)

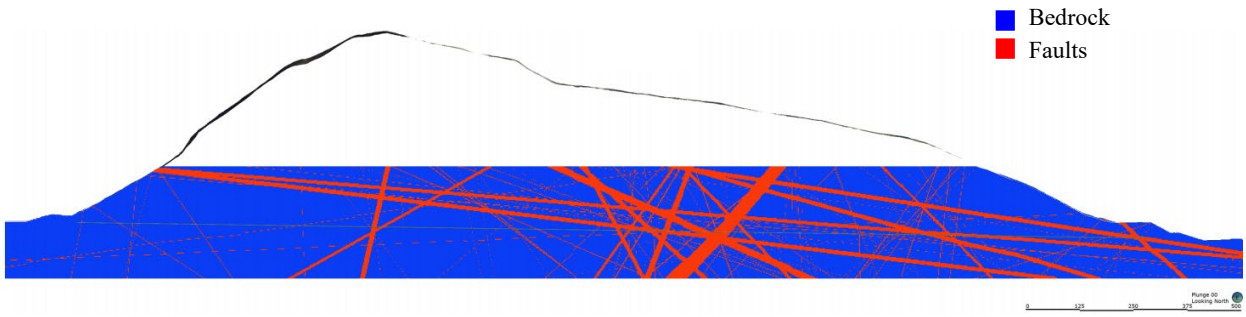

Figure 2.7: Geologic model showing the fault zone network to depth, based on probabilistic analysis of surficial and tunnel mapping during the construction of the pilot bore (Alexander, 2022).

2.6.3 Joints

2.6.3.1 Joint Spacing

Core samples[11] showed that the pieces of granite and metasedimentary rocks average 0.24 ft and 0.12 ft in length, respectively. Additionally, surface mapping showed that the average distance between fractures was 1.5 ft. Robinson & Lee (1964) suggested that the competency of granite was greater than that of the metamorphic rocks. Mattei (1965) indirectly proved that statement while logging the information obtained from the pilot bore. He observed that most of the self-supporting zones, or zones requiring minimal support, were sections constituted by SPG.

2.6.3.2 Joint Orientation

According to Richards (1963), four dominant orientations of closely-spaced joints were found in the research area: the maximum ranged from N80°E to S87°E dipping 75-85°N followed by N24°W, vertical; N83°W, 79°SE; and lastly N20°E, vertical. Furthermore, over 50% of these joint dips were greater than 70°, and more than 25% were larger than 80°.

In the pilot bore, Robinson et al. (1974) found three dominant joint orientations: the maximum was N75°E, 75°NW (parallel to the principal direction of faulting), then N45°W, 45°SW, and last N75°W, 65°SW. However, these sets represented less than 3% of all joints plotted (35 out of 1,179). It was concluded then that joints in the pilot bore struck in all directions and the average dip was about 45°. On the other hand, surficial samples showed two dominant joint orientations for the metamorphic rocks: N35°E, 45°SE, and N85°E, 85°SE. Additionally, most joints in granitic rocks struck NE with a dip average of approximately 70°SE, and joints with a dip angle greater than 45° were randomly distributed.

2.7 Groundwater

The water level in the core samples used by Richards (1963) appeared to be 50 ft. below the topographic surface at the east side of the Continental Divide, i.e., 730 ft. above tunnel grade or about 1500 ft. below the water table at the continental divide, as shown in Figure 2.8. However, the groundwater table data collected before and during the construction of the EJMT may be no longer applicable due to the several different parameters that might influence the face flow, including seasonal water availability, climate change, and the continuous drainage through the existing tunnels.

[11] The core sample (Drill Hole #2) was drilled in 1962 and used in several studies performed by Robinson & Lee from 1962 to 1974.

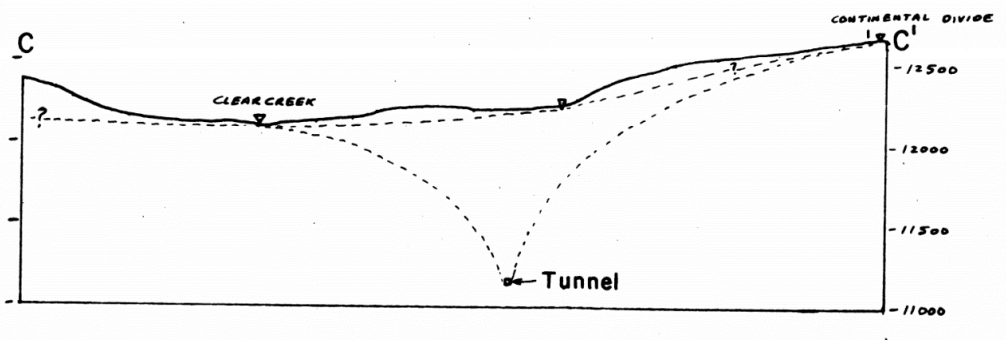

Figure 2.8: Illustration of the approximate location of the water table along the east side of the continental divide (Richards, 1963).

Similarly, the phreatic surface to the east of the continental divide (approximately a mile west of the west portal of the EJMT) ranged between 41.7 – 66.5 ft. in 1966[12]. Measurements taken at the same site between 2011-2015 showed that the depth to the groundwater table ranged between 16 – 23 ft. at the toe of the slope, 16 – 49 ft. on the westbound of I-70, and 82 – 98 ft. on the eastbound of I-70 (Wayllace, Lu, & Godt, 2017).

Since no bodies of ponded water are found on the surface above the EJMT, the springs originating at the tunnel site (Clear Creek and Straight Creek) may be related to permeable fracture zones that cut the bedrock terrain, which can reduce the total stress of the material due to an increase of the pore water pressure within joints.

[12] Field study performed by Kumar & Associates in 1966. Not a formally published document, but available in the literature.

CHAPTER 3:
THE INFLUENCE OF ROCK TYPE, LITHOLOGY, STRUCTURE, AND WEATHERING ON ROCK-SLOPE FAILURE MECHANISM

3.1 Overview

In general, slope stability depends upon the geological and geotechnical characteristics of the soil or rock that forms a hillslope. The Mohr-Coulomb or Hoek-Brown failure criteria (Hoek & Brown, 2019) are typically used to characterize the soil or rock mass strength and determine slope stability at a mass scale. However, in certain circumstances, the geological structure features of a rock mass like folds, faults, and joints control the rock mass behavior and determine the likelihood of slope failures (Fell, Stapledon, & Macgregor, 2012; Stead & Wolter, 2015). Accordingly, Duncan & Norman (1996) commented that the stability of rock slopes is more influenced by the structural fabric[13] than the properties of fractured rock masses like strength, permeability, and deformation. Therefore, determining the potential failure mechanism is crucial to correctly assess the method of analysis, i.e., slope stability analysis or kinematic analysis.

The possible landside types were determined using an updated version of the Varnes classification system (Varnes, 1954) proposed by Hungr, Leroueil, & Picarelli (2014). This new version defines 32 landslides ranging from rockfall to soil creep and considers the type of landslide-forming material, contrary to the original version.

In the following sections, the geologic characteristics of the material found in the vicinity of the EJMT, including the rock type, lithology, structural discontinuities, weathering degree, and rock mass quality, were analyzed to understand their effect on slopes stability and to determine possible landslide types where the prospective tunnel entrance could be placed.

3.2 Rock Type

During the construction of the EJMT, the SPG showed overall higher competency than the ISF (Mattei, 1965). Therefore, it seems the rock type could have some impact on the overall stability of the slope.

Intact SPG and intact ISF have similar strengths. However, the competency of ISF in the research area seemed largely affected by significant faulting and weathering rather than material strength.

[13] Structural fabric refers to a set or repetitive members of a particular defect (Duncan & Norman, 1996).

Therefore, slope failure is likely to occur in areas with higher content of ISF than SPG, i.e., east of the continental divide.

Based solely on the rock type, it is unclear what mechanism of failure these rock types would show. According to Terzaghi (1962), the critical slope angle for rock slopes with a random joint pattern (like the SPG) is approximately 70°. However, the slopes to the east and west of the continental divide are, on average, less than 45°; therefore, rockfalls or rock avalanches are unlikely to occur.

3.3 Lithology

Lithological boundaries between different rocks and soils usually result in changes in geomechanical properties. Alexander (2022) developed a lithological map using the information collected during the excavation of the pilot bore, which shows the three primary materials in the area: ISF, SPG, and dikes (see Figure 3.1). Note that this model assumed rocks with more than 50% SPG are only constituted of granite, and rocks with more than 50% ISF material are considered pure metamorphic rock. This simplification is somewhat radical, but the rapidly changing geologic conditions in the area would have made it practically impossible to model otherwise.

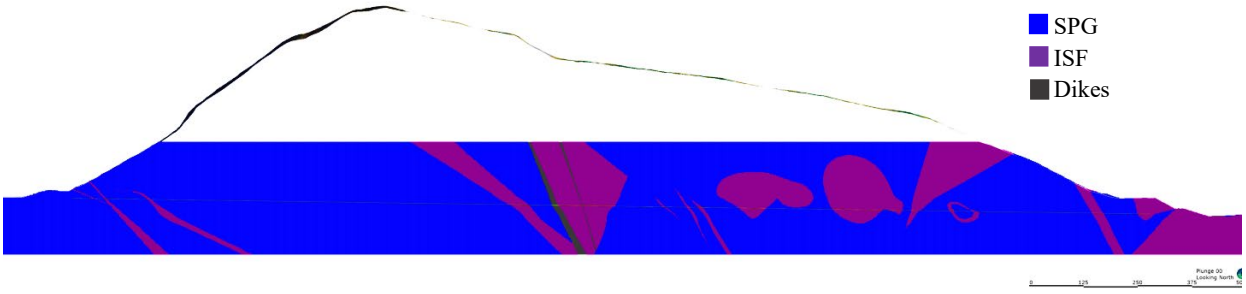

Figure 3.1: Geological model showing the lithological boundaries around the EJMT based on pilot bore mapping (Alexander, 2022).

Augite diorite dikes in the research area are gently fractured and unaltered, i.e., mainly intact rock. These dikes could potentially form groundwater barriers, decreasing the effective stress of nearby permeable material and causing instability. Considering the dikes are located about a mile into the mountain from the east portal, it is more likely they present a problem during the excavation of the tunnel bores than affect the stability of the slopes on both sides of the continental divide.

Another lithological boundary in the area is the contact zones between the SPG and the ISF material. However, the metasedimentary rocks are embedded in the granite; therefore, there is no sharp contact between the two that could result in sliding (see Section 2.4.2). Even if the contact zones are assumed to be sharp as Alexander modeled them, no clear stratigraphy was observed, and no planes were

daylighting on the slope faces. Therefore, a relationship between lithology and a specific failure mechanism could not be inferred.

3.4 Structural Discontinuities

3.4.1 Bedding

According to the geologic interpretations found in the literature (see section 2.4), there is no presence of sedimentary rocks in the research area; therefore, no further analysis will be made regarding failure due to bedding planes.

3.4.2 Foliation

According to Fell, Stapleton, & Macgregor (2012), foliated metamorphic rocks generally have a pronounced cleavage or planar foliation. Additionally, schists may present shear planes parallel to the foliation orientation and across the foliations at angles < 20°. Moreover, these defects are usually the initiating failure surface of landslides in schistose rocks such as those of the ISF.

Alexander (2022) analyzed 23 samples, including historical and current samples of ISF. Seven failed along the foliation, and 17 failed across the foliation. According to these results, slope failure at the east side of the continental divide, where most of the ISF deposits are located, may be related to cross-cutting faults on the more schistose rocks of the ISF. Accordingly, Alexander commented that structural weakness along the foliation planes might be expected.

Although laboratory testing may suggest that rock failure is likely to occur across the foliation, it needs to be extrapolated to the rock mass and the structural fabric that could generate instability. The foliation of the metamorphic rock has been extensively modified from the original parallelism (see Section 2.6.1), implying that the foliation of the ISF rock mass, if still present, does not describe a regional trend, and it might be more of a localized feature.

Robinson et al. (1974) stated that the foliation of the SPG was not a plane of weakness. Hence, the likelihood of mass failure of either the ISF or the SPG due to foliation would be minimal.

3.4.3 Faulting

Faults play an essential role in slope analysis, foundation design, and tunneling construction due to their association with sheared rock, usually characterized by small friction angles and higher permeability. The sheared rock found during the construction of the EJMT presented a gradational distribution of sizes, i.e., the rock size at the contacts ranged from less than 0.1 inches to 1.0 inches, confined by slickenside shear planes, followed by rock crushed to a coarse to fine sand (Miles & Mattei, 1965). Additionally, alteration of the smaller grains was also common producing fault gouge. These

shredded and altered materials were significantly weaker than the intact rock, which could result in potential planes of failure.

According to the information provided in Section 2.7.2, the rock mass at the research site was highly fractured and extensively altered along faults and shear zones, particularly on the east side of the continental divide. Furthermore, near the east portal, most faults were steeply dipping or dipping in the opposite direction than the slope face, except for two main faults near the slope surface (refer to Figure 2.7, pg. 13). However, these faults do not daylight the slope face (cut the slope at a shallower angle than the slope angle); hence it is improbable they may cause some degree of instability of the slope or even failure.

3.4.4 Joints

The joint spacing played a significant role during the construction of the pilot bore. Several sections of the tunnel presented a joint spacing of 0.1-0.5 ft. or less, which required maximum support to prevent a collapse. Although the effect of joint spacing on tunnel reinforcement relates differently to the effect it could cause on slope stability, there is a common factor, the strength of the rock mass. As the rock block size decreases, the strength of the rock mass also decreases (Hoek , Carranza-Torres, & Corkum, 2002). In general, metamorphic rocks in the research area had a smaller length than SPG (see section 2.6.3.1) which could result in areas of weakness causing instability.

Another important consideration in terms of slope stability is the joint orientation. The joints in intact granite are typically parallel to the ground surface forming exfoliating sheets parallel to the slope, and slope failures may occur through these fractures (Fell, Stapledon, & Macgregor, 2012). However, Robinson et al. (1974) determined that joints at the tunnel level struck in all directions with an average dip angle of 45^{o,} and the surface joints trended NE with a dip angle of at least 45^{o} (see section 2.6.3.2). In other words, joints in the research area did not show general parallelism to the ground surface, which could result in planes of weakness.

3.5 Weathering

Weathering usually begins at the ground surface and continues through sheet joints, tectonic joints, and faults, reducing the size of the relatively rectangular joint blocks to smaller, rounded forms separated by coarse weathered material. Weathered rock has considerably less strength than intact rock due to the reduction in strength parameters (Hoek & Brown, 2019). Additionally, the permeability will gradually increase as the rock blocks reduce in size and approach a soil-like grain distribution which might result in a significant reduction in total stress as pore water pressure builds up.

The surficial deposits in the upper slopes of the research area were primarily broken-weathered rock fragments that have accumulated on the hillslope. Similarly, the ISF was highly fractured, incompetent, weathered, and altered in a significant portion of the tunnel (Mattei, 1965). Therefore, the gradational weathered rock profile towards the ground surface and the rise of the water table during spring and summer could negatively impact the stability of the slopes around the east portal of the EJMT.

Granitic rocks are generally strong and relatively resistant to decomposition. However, weathering could occur in fault and shear zones and along joints, resulting in planes of weakness. Highly-weathered granite rock has a lower bulk density and shear strength than intact granite (Matsuo & Yamashita, 1968). Furthermore, it has higher permeability and virtually no joint cohesion making it highly susceptible to failure (Durgin, 1977).

The typical failure mechanism for fresh granite (<15% weathered rock), granite boulders (15-85% weathered rock), and decomposed granite (>85% weathered rock) are rockfalls, rockfalls avalanches, and debris, respectively (Durgin, 1977). Rockfalls usually result from localized structural failure, whereas rockfall avalanches and debris are strongly influenced by variations in the pore pressure.

During the construction of the EJMT, Mattei (1965) noted that fresh SPG was competent, but its strength was considerably reduced as it got faulted, altered, or weathered. On the other hand, the ISF showed less resistance to weathering and decomposition, and its strength was highly compromised. Therefore, based on an observational assessment of the material in the vicinity of the EJMT, the author believes that the most likely failure mechanisms involving SPG are rockfalls or rockfall avalanches, especially to the west of the continental divide. Conversely, rotational to translational to compound-complex sliding is more likely to the east of the continental divide, where a higher concentration of ISF can be found.

3.6 Mechanism of Sliding of the Loveland Basin Landslide

In 1972, a geophysical investigation was performed in the area to determine the morphology of the Loveland Basin landslide (Robinson, et al., 1972). Based on resistivity and seismic data, the slip surface was estimated to describe the shape shown in Figure 3.2.

Robinson et al. (1972) classified the Loveland Basin Landslide as a composite slide, where slump features were found in the upper part, and debris sliding and earthflows were located primarily towards the base. Although the landslide consisted of varied units moving at different rates, they most likely depended on each other.

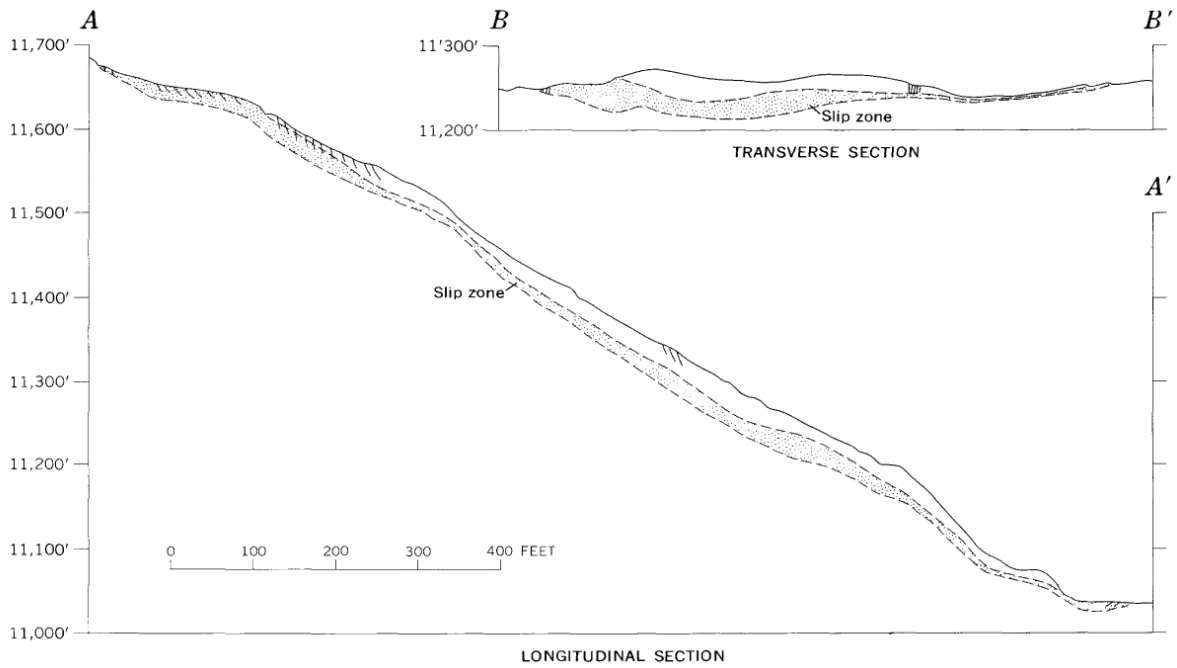

Figure 3.2: Longitudinal A-A' (Northwest-Southeast) and transverse B-B' (Northeast-Southwest) sections of the Loveland Basin Landslide (Robinson, et al., 1972).

According to the modified Varnes classification (Hungr, Leroueil, & Picarelli, 2014), a rock slump (or rotational rockslide) is a mass of weak rock that slides along a rotational rupture surface that is not structurally controlled. Furthermore, a prominent scarp, back-tilted bench at the head, and limited internal deformation are typical characteristics of these types of landslides. In rotational slides, water can accumulate on the slump's head due to the often-backward tilting of the slide or other irregularities, keeping the slide continuously wet and turning the slide into self-perpetuating areas of instability. On the other hand, debris slides consist of sliding of granular material where the movement is controlled by shallow, pre-existing structural planes parallel to the ground. Various material gradations are present in these slides, including colluvium and weathered soil.

3.7 Mechanism of Sliding in the vicinity of the EJMT

According to the information provided earlier in this chapter, it can be expected that :

1) Joints, fault networks, and weathering degree strongly influence rock slope behavior due to the significant reduction in the rockmass strength.
2) Rock type, lithology, and foliation would have little to no impact on any possible failure mechanism in the research area.
3) If failure would occur in the vicinity of the EJMT, a behavior similar to the Loveland Basin landslide could be expected, i.e., complex but not structurally controlled. Especially for the slopes to the east of the continental divide where there is moderate to highly weathered ISF.

Rockfall, rock wedge, and minor rock planar slides are possible on the west side of the continental divide. However, there would most likely be localized or single detachments from the outcrops above the west portal. Although this type of landslide could be devastating, it would probably not affect the integrity of the new or current tunnel bores. The study of these failure modes is beyond the scope of this research. The author suggests performing a kinematic analysis in any problematic joint or set of joints found in the area after detailed rock outcrop mapping.

The shallow faults near the slope face east of the continental divide (mentioned in section 3.4.3) are complicated to analyze because of the high uncertainty about their exact location, dimension, and orientation. Although they are an inherent point of weakness on the rock mass, none of the faults seemed to daylight on the slope, suggesting that the development of a failure plane through these features is improbable.

Since there are no particular features in the rock mass that suggest failure would occur through a particular slip surface. It is necessary to analyze the stability of the slope as a whole. Limit equilibrium and finite element methods were used for this purpose and explained in detail in the following chapter.

CHAPTER 4:
FUNDAMENTALS CONCEPTS, METHODOLOGIES OF ANALYSIS, INPUT PARAMETERS, AND THE INFLUENCE OF TUNNELING ON SLOPE STABILITY

4.1 Fundamental Concepts

Natural and artificial slopes are subjected to two types of forces: driving and resisting forces. When driving forces overcome resisting forces, the slope is considered unstable. Gravity is the main driving force, but several other factors, such as slope angle, water content, material, and human activity, contribute to its effect. On the other hand, the resisting forces depend on the shear strength of the soil, τ, which is usually expressed by the Mohr-Coulomb failure criteria as follows:

$$\tau_f = c + \sigma_n \, tan\emptyset \tag{4.1}$$

where c is the cohesion and $\emptyset$ is the internal friction angle expressed in terms of stresses, and σ is the total stress on the failure surface. It should be noted that the shear strength parameters (c and $\emptyset$) are not intrinsic properties since they depend on various factors such as void ratio, structure of the soil, effective stress, loading, and sample disturbance (Janbu, 1973). Therefore, obtaining reliable shear strength data is crucial for slope stability analyses.

Slope stability analysis compares the actual shear stress, τ, developed along the most likely failure surface with the shear strength of the soil and quantifies it by the factor of safety, F (Duncan, Wright, & Brandon, 2014) as follows:

$$F = \frac{\tau_f}{\tau} = \frac{c + \sigma_n \, tan\emptyset}{\tau} \tag{4.2}$$

When $F \leq 1$, the slope is in a state of impending failure. During a slope stability analysis, several slip surfaces are evaluated to find the critical slip surface with the minimum factor of safety.

A failure condition can be reached by decreasing the shear strength of the soil, increasing the shear stress, or both. Some of the mechanisms through which the shear strength of soils can decrease include:

- Increased pore water pressure (reduced effective stress)
- Cracking and swelling (increase in void ratio)
- Slickensides (frictional polishing of rocks at both sides of a fault, i.e., reduced friction angle)

- Decomposition of clayey rock fills (stable-compacted clay fill may lose its strength as it reverts to chunks of disaggregated clay particles when wetted by infiltration)
- Creep under sustained loads
- Weathering

On the other hand, the processes that lead to an increase in the shear stresses include:

- Applied external loads
- Increase in weight due to a larger water content
- Excavations of the slope toe (alleged trigger of the Loveland Basin Landslide)
- Reduction in ponded water level at the base of the slope (decreased hydrostatic pressure)
- Seismic effects

Generally, slope instability is caused by the simultaneous action of several of these mechanisms, and failure occurs due to a trigger that sets the soil mass in motion that was already in a state of impending motion.

4.2 Methodologies of Analysis

4.2.1 Limit Equilibrium Formulations

According to Hooke's law, the soil properties in the theories of equilibrium of elasticity are expressed in terms of stress-strain ($\sigma = E\varepsilon$). However, due to the inability to obtain an adequate stress analysis in the sliding soil mass to express the equilibrium theories of plasticity, it is necessary to perform a limiting equilibrium analysis (Morgenstern & Price, 1965). The factor of safety is calculated by an iteration process assuming an initial value of F and then calculating the corresponding shear stress, τ, until equilibrium is achieved according to the following expression:

$$\tau = \frac{\tau_f}{F} \tag{4.3}$$

Notice that the factor of safety will reduce the shear strength until a state of impending motion is reached, i.e., limiting equilibrium condition. Therefore, combining equations 4.1 and 4.3, the shear strength can be expressed as follows:

$$\tau_m = \frac{c}{F} + \sigma_n \frac{tan\emptyset}{F} \tag{4.4}$$

$$= c_m + \sigma_n tan\emptyset_m \tag{4.5}$$

where

τ_m is the mobilized shear strength

$c_m = \frac{c}{F}$ is the mobilized cohesion

$\emptyset_m = \tan^{-1}\left(\frac{\tan\emptyset}{F}\right)$ is the mobilized friction angle

This expression indicates that only a portion of the frictional and cohesive forces has been mobilized so that the soil is not in a state of failure on the assumed failure plane. It is worth noting that this concept is mathematically similar to the strength reduction technique discussed later in this chapter.

Several limit equilibrium methods to determine slope stability have been developed during the last century (Taylor, 1948; Frohlich, 1953; Fellenius, 1936; Bishop, 1955; Morgenstern & Price, 1965; Spencer, 1967; USACE, 2003). In general, two procedures are used to approach static equilibrium analyses:

1) Considering equilibrium for a single free-body (entire soil mass) delimited beneath by an assumed slip surface and above by the surface of the slope or,
2) Dividing the soil mass into slices and solving the equilibrium equations for each slice.

It is worth noting that single free-body procedures satisfy complete static equilibrium only by assuming a particular shape of the slip surface. A summary of some of the most popular procedures developed in the last decades is shown in Tables 3 and 4.

All the methods reviewed up to this point are based on simple slip surface shapes (plane or circular). However, failure surfaces are often more complex, following zones of relatively weak soil or weak interfaces between soil and other materials. Furthermore, none of these methods satisfy all equations of static equilibrium (forces and moment equilibrium). According to Morgenstern & Price (1965), this problem is related to the method itself rather than to the equations, which are mathematically correct.

Table 4.1: Summary of most important methods proposed in the literature for slope stability analyses using single free-body procedures indicating the assumptions made, the expression for the factor of safety, special cases, and applications.

	Method	Assumptions	F	Application
Single free-Body Procedures	Infinite Slope (Taylor, 1948)	▪ Slope of infinite extent, i.e., the depth of slip surface is slight compared to the lateral extent of the slope. ▪ Slip surface parallel to slope face.	$F = \frac{c' + (\gamma z \cos^2 \beta - u) \tan \emptyset'}{\gamma z \cos \beta \sin \beta}$ where, z =depth of the shear plane (measured vertically). β = inclination of the slope to the horizontal.	**Applications:** ▪ Non-plastic silts, sand, gravel, and rock fill where $c' = 0$. ▪ Shallow slopes where the stratigraphy limits the depth of the slip surface by a firmer stratum. **Limitations:** ▪ Only applicable for cohesionless materials, except for soils with curved Mohr failure envelopes that pass through the origin.
	Logarithmic Spiral (Frohlich, 1953)	▪ Finite slope. ▪ A logarithmic spiral defines the slip surface.	Logarithmic Spiral equations are relatively complex for hand calculations due to the assumed shape of the slip surface (Duncan, Wright, & Brandon, 2014). The Swedish Circle Method may be considered a special case of the Logarithmic Spiral Method because, at $\emptyset = 0$, a logarithmic spiral becomes a circle.	**Applications:** ▪ Theoretically, it is the best limit equilibrium procedure for analyzing homogeneous slopes. ▪ Software for designing reinforced slopes using geogrids, soil nails, and others. **Limitations:** ▪ Logarithmic spiral equations are too complex for hand calculations (best suited for computer programs).
	Swedish Method of Circles or SCM[14] (Duncan, Wright, & Brandon, 2014)	▪ Finite slope. ▪ A circular arc defines the slip surface. ▪ Sum of moments about the center of the circle. ▪ Undrained soil conditions ($c = c_u$ and $\emptyset = 0$).	$F = \frac{c_u L R}{W D}$ R: radius of the circle W: weight of the soil mass above the slip surface D: moment arm of the soil mass weight L: length of the slip surface c_u: undrained cohesion	**Applications:** ▪ Undrained cohesive soils ▪ Relatively thick zones of weaker materials where a circle can approximate the slip surface. **Limitations:** ▪ Several slip surfaces need to be assumed to find the minimum value of the factor of safety.

[14] The SCM apparently was formally introduced by Fellenius in 1922 (Duncan, Wright, & Brandon, 2014) but the suggested article *(Staten Jarnjvagars Geotekniska Commission)* could not be found and therefore, it was not cited.

Table 4.2: Summary of most important methods proposed in the literature for slope stability analyses using the method of slices indicating the assumptions made, the expression for the factor of safety, special cases, and applications.

	Method	Assumptions	F	Characteristics
Slices Procedures for Circular Slip Surfaces	Ordinary Method of Slices (OMS) (Fellenius, 1936)	▪ Circular slip surface. ▪ Sum of moments about the center of the circle. ▪ The resultant of the interslice forces act perpendicular to the normal force. ▪ No interslice shear forces. ▪ Driving forces are due only to the self-weight of the soil mass.	$$F = \frac{\sum[c'\,\Delta l + (W\cos\alpha - u\Delta l\cos^2\alpha)\tan\emptyset']}{\sum W\sin\alpha}$$ where, Δl = length of the bottom of the slice. α = inclination of the bottom of the slice. u = pore pressure **Submerged or partially submerged slope:** $$F = \frac{\sum\{c'\,\Delta l + [W\cos\alpha + P\cos(\alpha-\beta) - u\Delta l\cos^2\alpha]\tan\emptyset'\}}{\sum W\sin\alpha - \frac{\sum M_P}{R}}$$ where, P = resultant water force perp. to the top of the slice. β = inclination of the top of the slice. M_P = water force moment about the center of the circle R = radius of the circle.	**Applications:** ▪ Non-homogeneous slopes and $c-\emptyset$ soils. ▪ Convenient for hand calculations as it permits a direct calculation of F (i.e., no iteration needed). **Limitations:** ▪ Inaccurate for effective stress analyses with high pore pressures. ▪ Does not account for the interslice shear forces. ▪ Does not satisfy the equilibrium of forces in either the vertical or horizontal directions. ▪ Moment equilibrium is satisfied for the entire soil mass but not for individual slices.
	Simplified Bishop Method - Extended (Bishop, 1955)	▪ Circular slip surface ▪ Only considers normal interslice forces but ignores interslice shear forces. ▪ Sum of moments about the center of the circle. ▪ Driving forces are due only to the self-weight of the soil mass	$$F = \frac{\sum\left[\frac{c'\Delta l + (W - F_v - u\Delta l\cos\alpha)\tan\emptyset'}{\cos\alpha + \frac{(\sin\alpha\tan\emptyset')}{F}}\right]}{\sum W\sin\alpha - \frac{\sum M_n}{R}}$$ where, F_v = equivalent resultant force of all vertical components of all of the known forces except the slice wight. M_n = net moment due to all known forces except the weight. *Notice that for $\emptyset = 0$, the Logarithmic Spiral, Swedish Circle, OMS, and MMS give the same value of F.*	**Applications:** ▪ Non-homogeneous slopes and $c-\emptyset$ soils. ▪ Improved results over the OMS for effective stress analyses with relatively high pore pressure. ▪ Results are usually within a 5% difference of rigorous methods. **Limitations:** ▪ It is a trial-and-error method, as the term F is on both sides of the equation. Hence, it must start with a guess for F (It is reasonable to start with the value of F obtained from the OMS). ▪ Horizontal forces equilibrium is not satisfied.

The Simplified Janbu method and the U.S. Army Corps of Engineers method offer a slightly more advanced procedure for slopes with non-circular slip surfaces; however, the moment equilibrium equation remains unsatisfied. More rigorous limit equilibrium analyses, i.e., methods that can be utilized for slopes with non-circular slip surfaces and satisfy all the equilibrium conditions are available, including the Spenser and Morgenstern-Price method. However, computer processing is required to solve the proposed equations.

Although Limit Equilibrium (LE) methods give reasonable solutions for the factor of safety, there are several limitations inherent to the procedure itself, which are listed below:

1) The lack of knowledge to obtain the actual stress distribution along the potential slip surfaces, and therefore, a stress-strain relationship for plastic deformation.
2) Localized shear stress concentrations are not captured (for shallower slip surfaces, the stress contour is closer to the slope surface under the toe). Instead, the normal stress distribution is derived primarily from the overburden weight.
3) An intrinsic error is associated with the number of assumptions needed to solve the equilibrium conditions. Particularly assumptions regarding the interslice forces direction.
4) The factor of safety is a single value representative of the whole slipping soil mass. However, the local factor of safety can be smaller or greater than the global value.
5) Iterative convergence to a single value of the factor of safety is challenging when the slip surface contains steep sections, jumps, and complex geometries.
6) Complex procedure to treat external forces applied to the soil mass.
7) The stiffness of the slope material is not considered. Hence, the margin of safety is reduced.

Numerical analyses are an alternative to overcome these problems, which offer accurate, robust, and versatile procedures to perform slope stability analysis. These procedures include methods like the finite element method (FEM), finite difference method (FDM), boundary element method (BEM), and discrete element method (DEM). The FEM has become one of the most preferred numerical methods in the geotechnical engineering community because it is relatively simple and considers the slope's geometry, the forces acting on the slope, the material properties, and the strength parameters.

4.2.2 Numerical Methods – Deterministic Approach

Typically, slope stability problems can be solved using LE-based software like SLOPE/W from GeoStudio. However, many slopes have highly irregular slope profiles, a complex lithology, or are affected by structural discontinuities such as joints, faults, and bedding planes. Precise representation of these scenarios can be accomplished using numerical methods, which involve diverse types of modeling approaches: continuum, discontinuum, and hybrid.

Continuum modeling is generally suitable for analyzing soil slopes, massive intact rock, or heavily jointed rock masses through the finite difference or finite element method. The FEM was the preferred analysis method for this research, using programs like RS2 and RS3 from Rocsience. This software has grown in popularity in the last years, particularly for underground engineering design and slope stability analysis, due to the intuitive workflow and user-friendly interface.

Griffiths & Lane (1999) combined the FEM with the shear strength reduction technique (SSR) to expand this technique to slope stability analysis. In this method, the factor of safety is represented by the Strength reduction factor (SRF), which is the ratio between the actual and the model strength at the stability limit. According to Kaya et al. (2017), the main advantage of the FEM-SSR method is that there is no need to make a priori assumptions regarding the shape or location of the slip surface. Failure occurs "naturally" when the applied shear stress surpasses the shear strength of the soil mass (Griffiths & Lane, 1999). A list of other advantages of the finite element method include:

1) There is no need to make assumptions about interslice forces since the slice approach is not used in the FEM.
2) Deformations due to applied external stresses, i.e., a stress-strain relationship, can be determined if actual soil compressibility data is available.
3) The computed stresses along the soil mass are much more reliable than those from LE methods. Additionally, localized shear stress concentrations are indirectly considered in the analysis.
4) It is possible to perform progressive failure monitoring until overall shear failure is reached.

Perhaps the "higher complexity" of this method and the necessity for practicing geotechnical engineers to learn the ins and outs of the finite element programs pushed back its application in the field. However, there are several situations where a slope stability analysis would benefit from a FE treatment, such as slopes with complex geometries or soil properties variations that are not covered by classic procedures.

Generally, FEM use elastic-perfectly plastic constitutive models to describe soil or rock mass behavior (Griffiths & Lane, 1999). The material is assumed to behave elastically while the model generates normal and shear stresses at all Gauss points (nodes) within the mesh. Then, these stresses are compared with failure criteria models like the Mohr-Coulomb or Hoek-Brown failure criterion. The material is assumed to remain elastic where the stresses are below the failure envelope and yield where the stresses match or surpass the shear strength of the soil or rock. Failure occurs when a sufficient number of Gauss points have yielded to allow a failure mechanism to develop.

Finite element analysis is fundamentally based on stress distribution across a mesh. Therefore, the Mohr-Coulomb criterion shown in equation 4.1 is better expressed in terms of principal stresses, as follows:

$$F = \frac{\sigma'_1 + \sigma'_3}{2} sin\,\emptyset' - \frac{\sigma'_1 - \sigma'_3}{2} - c'\,cos\,\emptyset' \qquad 4.6$$

where σ'_1 and σ'_3 are the major and minor principal effective stresses, respectively. Thus, the behavior of soil or rock mass can be determined as follows:

- $F < 0$ stresses inside failure envelope (elastic)
- $F = 0$ stresses on failure envelope (yielding)
- $F > 0$ stresses outside failure envelope (yielding and must be redistributed)

Although different input parameters are used to model a particular scenario, the most critical parameters for slope stability analysis using finite elements are similar to those used in LE methods, i.e., unit weight γ, the shear strength parameters c' and $\emptyset'$, and the geometry of the problem (Griffiths & Lane, 1999). Then, the forces generated by the self-weight of the soil are obtained by multiplying the area of each element and the total unit weight of the soil. The net vertical force is then consistently distributed to all the nodes and assembled into a global gravity force vector that is applied to the FE mesh to generate the initial stress state of the problem. Finally, the factor of safety (F) is defined as the factor by which the original shear strength parameters must be divided to cause a slope failure, i.e., the strength reduction factor (SRF). At failure, the value of F obtained from LE methods and the SRF obtained from FE methods are virtually identical. During the rest of the document, both concepts will be referred to as factor of safety.

4.2.3 Probability of Failure

The methodologies presented in the previous sections correspond to deterministic approaches, i.e., the result is a singular value. In these methods, sensitivity analyses are the only way to integrate parameters uncertainty into the analysis. According to Duzgun, Yucemen, & Karpuz (2003), sources of uncertainty on input parameters for rock slope stability include:

1) Inherent variability
2) Statistical variability
3) Systematic variability

Inherent variability is associated with the natural heterogeneity of rock masses. Statistical variability occurs from limited sampling and laboratory testing and it is related to the mean and standar

deviation of a parameter. This type of uncertainty decreases as the number of samples increases. Systematic uncertainty results from the discrepancies between the laboratory and in situ conditions, due to factors such as scale, anisotropy, and water saturation. Since these are fixed conditions, additional sampling typically does not reduce uncertainty. A priori, it seems that the only alternative to decrease uncertainty of slope stability analyses is to perform numerous in-situ and laboratory sampling to increase the data universe and obtain minimal standar deviations for all input parameters. This is highly unpractical and economically unfeasible for most projects, though, the utilization of probabilistic methods for slope stability analyses permits a rational treatment of various sources of uncertainties.

Uncertainty is usually represented by the standard deviation (σ) or the unitless Coefficient of Variation (Vc or COV), determined as follows:

$$Vc = \frac{\sigma}{\mu} \tag{4.7}$$

where μ is the mean value of the parameter. Therfore, the higher the Coefficient of Variation, the higher the Probability of Failure (P_f).

For rock slope stability problems, there is a high uncertainty associated with the shear strength of discontinuities. Often, the strength of fractured rock with unfilled discontinuities is assumed to be provided completely by frictional forces. Some comprehensive statistical models for quantification and analysis of uncertainty involved in the estimation of friction angle by aggregating inherent variability, and statistical and systematic uncertainties within the first-order uncertainty analysis framework is available in the literature (Duzgun, Yucemen, & Karpuz, 2002; Duzgun, Yucemen, & Karpuz, 2003).

Probably one of the main reasons why probabilistic methods have not been widely used by the geotechnical community, is the lack of consensus about acceptable limits to characterize slope stability. In deterministic analsyses, a factor of safety of F = 1.3 and F = 1.5 are accepted minimal design values for temporary and permanent slopes, respectibly. However, these methods do not include treatment of uncertainties, which can lead to situations where slopes with higher factors of safety have higher probabilities of failure. According to the 2017 H. Bolton Seed Medal Lecture: Numerical Analysis of Stability and Risk in Highly Variable Soils, Dr. Griffiths stated that: “direct comparison between the Factor of Safety and the Probability of Failure is to be discouraged”.

A rigorous method of probabilistic geotechnical analysis in which nonlinear finite-element methods are combined with random field generation techniques was proposed by Giffiths & Fenton (2004). The random finite-element method (RFEM) fully accounts for spatial correlation and averaging properties in combination with all the benefits of the FE methods.

4.3 Input Parameters for Slope Stability Analysis

One of the most complicated tasks while using LE or FE methods to determine slope stability is to adequately characterize the properties of the rock mass to simulate a realistic behavior. The strength of jointed rock masses near the surface may be significantly reduced compared to intact rock due to faults, joints, and weathering. Therefore, intact rock properties are not applicable.

Rock mass classification systems provide an easy and intuitive procedure to account for geological features such as blockiness and weathering. Numerous rock mass classification systems have been developed in the last 60 years to assess the quality of rock masses, and many reviews and comparisons between these systems can be found in the literature. Rehman et al. (2018) recently published a complete literature review and summary of rock mass classification systems. In general, the three most widely used rock mass classification systems are the Rock Mass Rating (RMR) system, the Rock Mass Quality Index (Q-system), and the Geological Strength Index (GSI). The GSI considers the mechanical properties of a rock mass to be affected primarily by the block size of the rock mass and its condition, i.e., weathering and roughness. Additionally, it does not apply to structurally controlled failures, which would dominate the rock mass behavior. The author recommends referencing Hoek, Carranza-Torres, & Corkum (2002) for more information about the system.

Failure criteria like the H-B criterion incorporate intact rock and discontinuities into a yield model designed to estimate the mechanical properties of rock. This model uses the strength and deformation properties of intact rock, typically obtained from laboratory tests such as triaxial tests, and reduces them based on the GSI. As previously reported in the literature (Robinson & Lee, 1964; Richards, 1963; Mattei, 1965; Robinson, et al., 1974), the rock mass in the research area is highly faulted, weathered, and altered along joints, primarily to the east of the continental divide. A typical outcrop in the research area is shown in Figure 4.1.

Figure 4.1: Typical outcrop east of the EJMT showing extensive fracturing and weathering.

The geomechanical properties of the SPG proposed in Table 2 (pg. 10) correspond to those of the intact rock. The rock mass strength of the SPG was then determined by assigning a peak GSI (GSI_P) based on field observations. The residual GSI (GSI_R) was determined using the expression proposed by Cai, Kaiser, Tasaka, & Minami (2007):

$$GSI_R = GSI\ e^{-0.0134\ GSI_P} \quad 4.8$$

The laboratory test results of the ISF analyzed by Alexander (2022) showed significant scatter around the regression envelopes due to the wide variability of the rocks making up the ISF. The uncertainty in the rock mass properties was accounted for through a statistical analysis of 24 samples assuming the ISF as an isotropic material and reducing the M-C yield model to a single failure envelope. Since rock blockiness and weathering degree cannot be directly incorporated into the M-C criteria, further consideration must be taken for slope stability analyses using the geomechanical properties proposed for the ISF. For instance, a thorough sensitivity analysis of friction angle and cohesion should be performed to account for the reduction in strength of the rock mass compared to an intact rockmass.

4.4 Effect of Tunneling on Slope Stability

The interaction between underground excavations and slope stability is relatively complex because it may be influenced by the geological conditions, the tunnel structure design, the construction methods, and the construction in-time stability treatments (Zhang, Zhao, Xu, & Xu, 2017). Slope instability is a common issue at tunnel portals and underground constructions close to the face of a slope as the excavation work may cause a redistribution of stresses with local increases of the deviatoric stresses (Gattinoni, Consonni, Francani, Leonelli, & Lorenzo, 2019).

Underground work can be considered shallow when the disturbed area around the tunnel affects the ground surface, specifically when the overburden thickness is approximately less than four times the excavation diameter (Gattinoni, Pizzarotti, & Scesi, 2014). Shallow underground works are strongly affected by water inflows, which may cause weathering of the rock and soils. Additionally, they are strongly affected by the topography and surface loads, i.e., a reduction in the overburden pressure could cause a dissymmetrical stress distribution which may cause an irregular deformation phenomenon depending on the bedding arrangement and fracturing degree. Contrarily, deep underground works are not significantly affected by geomorphological conditions if they are not located in steep slopes, glacial valleys, or areas characterized by deep-seated landslides. The morphology of these terrains may still be affected even at great depths.

Since the geologic structure features of a slope cannot be changed, it may be wise to avert tunnel routes from unstable terrains. However, it is unrealistic to prevent all underground works from encountering such terrains and unpractical for urban design purposes. Therefore, adequately choosing the location of tunnels is perhaps the most critical design factor in minimizing the possibility of landslides.

4.4.1 Displacement Distributions

4.4.1.1 Displacement distribution induced by tunnel location

The displacement distribution of a slope against tunnel location for a fixed distance between the slip surface and the tunnel shows two different behaviors (Koizumi, Yokota, Date, & Fujisawa, 2010). First, tunnel excavations near the foot of a slope show a relatively similar displacement distribution to that of a slope without a tunnel, suggesting that a tunnel simply tends to accelerate movement at this particular location. Contrarily, tunnel excavations at the center and near the top of a slope tend to weaken the slope in the horizontal direction, resulting in a more complicated behavior.

Another parameter to consider is the distance between the slip surface and the tunnel. There is some agreement in the literature in terms of the shortest distance between a tunnel and the potential slip surface in order to minimize their interference, i.e., the location at which the plastic strain zone developed from the tunnel does not intersect with the slip surface (Koizumi, Yokota, Date, & Fujisawa, 2010; Causse, Cojean, & Fleurisson, 2015). Koizumi, Yokota, Date, & Fujisawa (2010) proposed that this distance range between 1.5 to 2.0 D, where D is the diameter of the tunnel bore. Similarly, Causse, Cojean, & Fleurisson (2015) stated that the slope surface displacement rate is significant for tunnels located less than 1.5 D from the slip surface.

According to Vlachopoulos & Vazaios (2015), the horizontal translation into the slope of tunnel bores relative to their original design location has a minimal positive influence on the stability of the slope. From their analysis, the original position of the tunnels resulted in a factor of safety of 1.15, and a horizontal translation of 2.5D and 4D increased the factors of safety by 1.7% and 2.6%, respectively. This result might be related to the fact that the slope angle used for their study was only 21°. Thus, since the run was much greater than the slope's rise, the overburden pressure did not change significantly from one point to another; therefore, the stresses developed along the slope were similar at varied horizontal locations. The authors above also studied the influence of a vertical translation on the stability of a slope. The vertical translations of 2.5D and 4D increased the factors of safety by 2.6% and 5.2%, respectively. This indicates that a vertical translation of a tunnel (increasing depth) would positively impact the stability of the slope since higher overburden fosters a stress redistribution or arching effect instead of acting as a deadweight over the tunnels. However, the increase in stability was still minimal. It is of the opinion of the author that these results cannot be easily extrapolated because the original location of

tunnels is a specific parameter for each project. Instead, a universal reference point such as the slope face should have been used to maximize the applicability of their research.

4.4.1.2 Displacement distribution induced by tunnel excavation

According to Wang, Zeng, Xu, & Feng (2017), the first excavation step into the slope may cause a significant horizontal displacement of the slope surface, which tends to converge as the excavation of the following steps continues, i.e., the horizontal displacement decrease as the tunnel excavation is further into the slope. Similarly, the vertical displacement, mainly concentrated at the top of the tunnel, tends to decrease as the excavation moves further into the slope. Additionally, an uplift phenomenon of the soil at the bottom of each step may occur due to the surrounding soil pressure.

4.4.2 Tunnel Portals

According to Wang (2019), a tunnel portal is the section of a tunnel where the distance from the slope face to the upper part of the tunnel bore is approximately 1 to 2 times the tunnel's diameter, as shown in Figure 4.2.

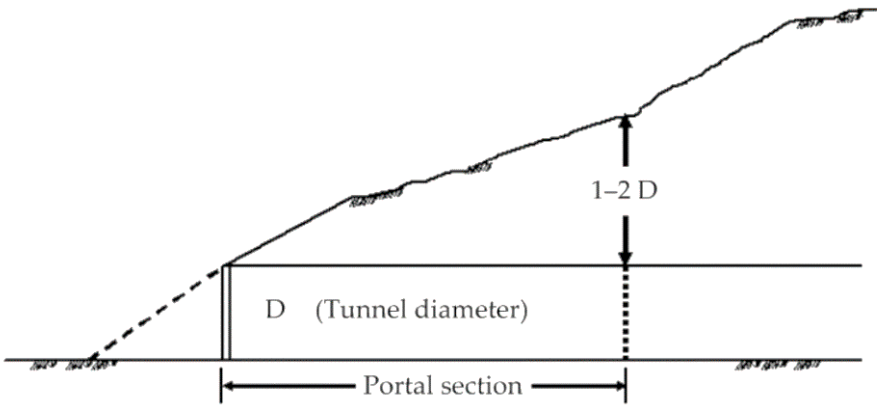

Figure 4.2: Schematic diagram for a standard portal section range (Wang I. , 2019)

Tunnel portals excavated in rock masses can experience problems of compression, alteration, or fracturing phenomena undergone by the rock. Additionally, if the excavation of tunnel portals takes place in loose material such as debris or glacial deposits with poor geotechnical properties, slope stability problems might be expected (Gattinoni, Pizzarotti, & Scesi, 2014). Regardless of the situation, ground stabilization would be required if the slope stability analysis recommends it.

Typically, tunneling projects start by cutting the slope to get as close as possible to competent rock and create an almost-vertical wall with enough clearance to fit the tunnel face. This phase of the

excavation process can easily get affected by landslides due to the removal of the slope toe, i.e., the resisting forces are reduced. Slope stability analysis would provide critical insight into the possible outcomes from this excavation phase and if reinforcement should be used. According to the Technical Manual for Design and Construction of Road Tunnels (U.S. Department of Transportation, 2009), tunnel pre-support is usually installed after the tunnel plaza has been cleared and the respective slope-cut support has been set up. The pre-support consist of a row of horizontal pre-spiling or grouted steel pipes of about 10 to 60 ft. in length based on the degree and depth of weathering. These elements are typically separated at 12-inch centers around the prospect tunnel opening, as shown in Figure 4.3. Additionally, a shotcrete collar should be installed around the tunnel perimeter and tied in with the protruding pre-support elements to provide stability to the ground in the vicinity of the tunnel.

Figure 4.3: Typical pre-support at a portal wall and shotcrete application for portal face protection (U.S. Department of Transportation, 2009).

As previously mentioned, the excavation of the access road to the east portal of the EJMT triggered the Loveland Basin landslide. As a result, the tunnel's alignment had to be changed, remediation measures had to take place to stabilize the slide, and several years of monitoring the terrain were needed to establish its safety. The Loveland Basin landslide could have been prevented by performing a throughout slope stability analysis during the design phase, construction, and further if needed. However, the author found no records of slope stability analyses in the area before the failure occurred.

According to the information provided in Chapters 2 and 3, it can be expected that the slope stability at the research site is strongly influenced by geological, meteorological, and hydrological factors, which can translate to slope instability and landslides. During the construction of the Pilot Bore, even good-quality rock needed some support. Therefore, it is reasonable to think that highly fractured, weathered, and jointed ISF, as the rock found near the prospect construction site, may require pre-support or ground stabilization for the construction of the new portals.

CHAPTER 5:
COMPUTER MODELS DEVELOPMENT

5.1 Overview

Computer models are used to solve complex slope stability problems. Despite some disadvantages between different software available, most allow determining the factor of safety of soil or rock slopes with a relatively good degree of agreement.

Based on the statistical analysis performed by Alexander (2022) to determine the geomechanical properties of the SPG and ISF, it could have been safe to assume that the properties of these materials were relatively reliable. However, the results proposed carried several assumptions to model the Mohr-Coulomb and Hoek-Brown failure criteria for the ISF and SPG, respectively. Thus, a sensitivity analysis was necessary to evaluate the effect of uncertainty on material properties. Other parameters considered that could cause a significant impact on slope stability included depth to groundwater table and snow loads. The values used in the sensitivity analyses, based on the standard deviation encountered by Alexander (2022), are shown in Table 5.1.

Table 5.1: Parameters used to perform sensitivity analyses of the slopes in the vicinity of the EJMT

Material	Parameter	Proposed Value	Range
ISF	$\emptyset'$ (degree)	37.5	24.4 – 45
	c' (MPa)	21.9	14.2 – 29.5
	Depth to GWT (ft)	-	0 – 85
	Snow Loads (MPa)	-	0 – 0.072
SPG	UCS (MPa)	179.6	89.8 – 179.6
	GSI_P	55	27.5 – 55

Note 1: The proposed values correspond to those reported in Table 2.2.
Note 2: $\emptyset'$ is the internal friction angle, c' is cohesion, GWT is groundwater table, UCS is the unconfined compressive strength, and GSI_P is the peak GSI.

Several computer models were developed for this research, including LE models to validate the results presented in the literature regarding the stability of the Loveland Basin landslide (see Table 1) and two-dimensional and three-dimensional FE models to analyze the stability of the slope east and west of the continental divide, respectively. A summary of the geotechnical interpretation performed and discussed in the previous chapters, and used to determine the most suitable Software for analysis, is shown in Figure 5.1.

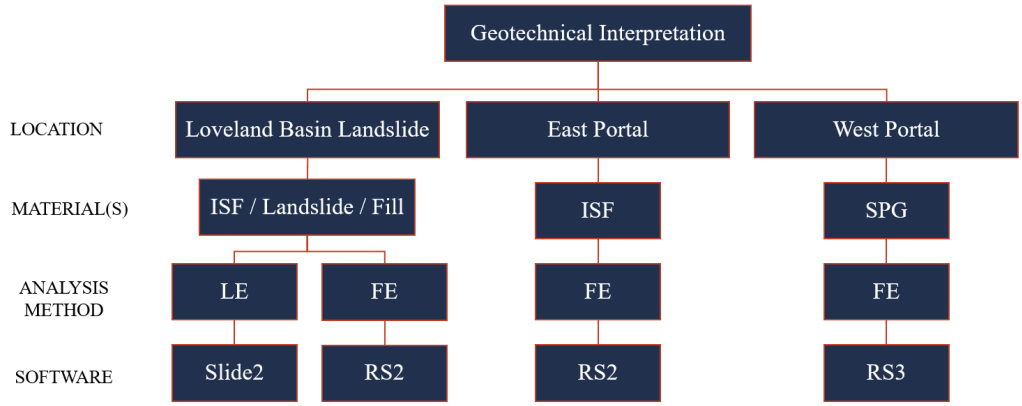

Figure 5.1: Summary of slope stability analyses based on location, material, failure criteria, analysis method, and software used.

5.2 Selection of Additional Tunnel Alignment

Alexander (2022) developed a geologic model and performed the engineering interpretations to determine feasible tunnel alignments for the new tunnel bores for the EJMT. The original data set resulted in 8,216 possible alignments from a selected number of possible portal locations. The initial filtering considered the following parameters:

- Tunnel grade was restricted from 0.5% to 2% to promote proper water drainage, ventilation, and traffic safety.
- Ground surface conflicts such as the slopes facing the west portal.
- Minimum distance with existing tunnel bores of at least the sum of the bore radius.

In subsequent data filtration, several other metrics were considered to determine the best alignments, including maximum depth, length, squeezing potential, and rock mass geologic features. Additional filtering was made based on the best alignment for different excavation methodologies. The highest scoring metrics for each of the proposed alignments are specified in Table 5.2, a summary of critical parameters of these alignments is shown in Table 5.3, and their approximate locations are shown in Figure 5.2.

Table 5.2: Highest scoring metric for the top seven alignments proposed by Alexander (2022)

Alignment No.	Highest Scoring Metrics
211	TBM constructability
243	Lowest rock mass class dispersion
2273	Shortest
2929	Shallowest mean depth
4495	Highest average rock mass class scores
5448	Highest cross score, RMR, Q, and D&B constructability
8131	Shallowest max depth

Table 5.3: Top six possible alignments for the new tunnel bore at the research site – Based on Alexander (2022)

	West Portal			East Portal						
Alignment No.	**Latitude**	**Longitude**	**Elevation (ft)**	**Latitude**	**Longitude**	**Elevation (ft)**	**Length (mi)**	**Max Depth (ft)**	**Mean Depth (ft)**	**Fault Zone Occurrence (%)**
211	39°40'33.12"N	105°56'4.82"W	11,342	39°40'26.86"N	105°54'21.82"W	11,338	1.50	1,290	584	29.9
243	39°40'11.52"N	105°56'41.39"W	11,434	39°40'26.69"N	105°54'17.38"W	11,325	2.07	1,273	646	44.0
2273	39°40'39.43"N	105°56'2.43"W	11,290	39°40'40.68"N	105°54'22.28"W	11,178	1.43	1,358	722	30.9
2929	39°40'11.50"N	105°56'41.12"W	11,431	39°40'41.38"N	105°53'25.42"W	11,127	2.84	1,375	499	48.3
4495	39°40'46.12"N	105°56'15.76"W	11,209	39°40'51.05"N	105°54'9.29"W	11,111	1.80	1,401	715	25.0
5448	39°40'49.85"N	105°55'58.21"W	11,302	39°40'58.11"N	105°54'5.23"W	11,337	1.62	1,171	656	0.0
8131	39°40'46.33"N	105°55'58.42"W	11,291	39°41'12.38"N	105°53'22.00"W	11,172	2.23	1,155	538	26.9

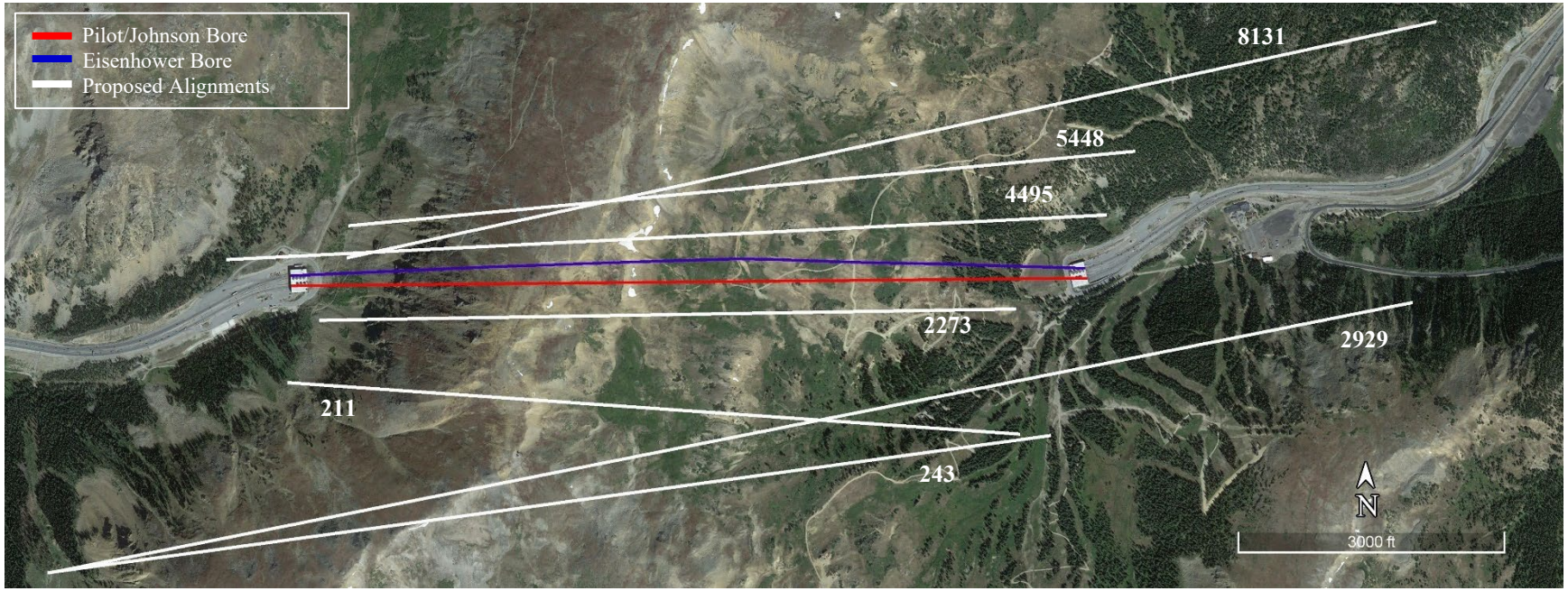

Figure 5.2: Approximate location of the top seven alignments for the additional bores of the EJMT proposed by Alexander (2022)

Of the seven best alignments, Alignments No. 2273 and 2929, i.e., the shortest and shallowest, might be considered the prime alignments to analyze from a purely economic standpoint. However, seeking a more favorable rock mass quality might result in higher excavation efficiency (Alexander, 2022). The east portals of alignments No. 211, 243, and 8131 would be located directly on protected areas according to laws 49 USC 303 and 23 USC 138, with the associated detailed regulations under 23 CFR 774. Thus, the construction of a tunnel within Loveland Basin Ski Resort dependencies would need significant legal efforts, and if approved, it would most likely disrupt recreational activities. Alignment No. 4495 showed the highest rock quality and lowest average elevation, i.e., only 88 ft above the current east portal. However, it intersects the Loveland Basin landslide, which could cause it to reactivate and potentially damage the existing bores. Alignment No. 5448 scored the highest in four metrics, including gross score, D&B-focused metrics, Q-based metrics, and RMR-based metrics. The favorable rock quality along this alignment and the fact that D&B will probably be the preferred excavation method suggests that Alignment No. 5448 is the most promising alignment. However, an access road would need to be built from I-70 to the proposed east portal. It is noteworthy that although alignment No. 5448 might be the most favorable alignment in terms of constructability, alignment No. 4495 might be the most economically efficient option since the elevation difference between the new and current portals would be minimal, i.e., no approximation road would be needed. However, a financial evaluation is out of the scope of this research.

In practice, the selection of Alignment No. 5448 or 4995 would necessitate a thorough slope stability analysis of the Loveland Basin landslide. Sub-surface explorations would be required to determine the ground properties and slip surface depth. The installation of inclinometers would be highly recommendable to determine if the landslide is dormant or if any movement is currently under motion. Finally, infiltration-induced instability should be considered due to the highly variable water table in the area. Since both of these alignments are likely to be selected, they were used as a point of reference to study the tunnel-slope interaction on the slopes in the vicinity of the EJMT.

5.3 Slopes East of the Continental Divide

5.3.1 East Portal

The relative perpendicular position of the east slope to the new tunnel bores suggested that plane strain conditions could be assumed, i.e., the principal strain in the direction of the tunnel alignment was constrained, resulting in zero strain along that plane. Therefore, numerical simulations were simplified using a 2-dimensional model. Critical parameters of the three main cross-sections selected for analysis (see Figure 5.6) are presented in Table 5.4.

Table 5.4: Critical parameters of the cross-sections selected for 2-dimensional analysis

	Top			Bottom			
Name	**Latitude**	**Longitude**	**Elev. (ft)**	**Latitude**	**Longitude**	**Elev. (ft)**	**Slope Angle (deg)**
A-A’	39°41'9.27"N	105°54'17.09"W	11,701	39°40'38.63"N	105°54'13.42"W	11,150	30
B-B’	39°41'11.02"N	105°54'11.56"W	11,583	39°40'40.21"N	105°54'8.15"W	11,116	45
C-C’	39°41'13.02"N	105°54'6.33"W	11,481	39°40'41.76"N	105°54'2.99"W	11,058	25

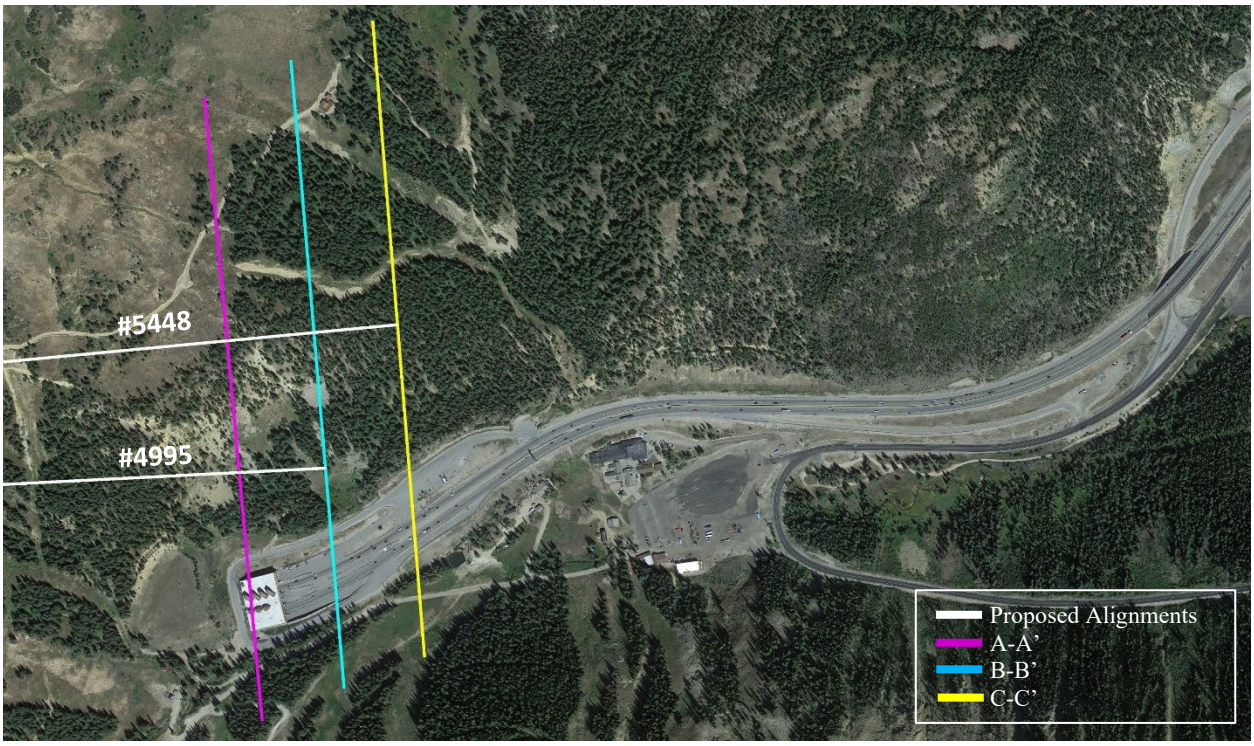

Figure 5.3: Slopes to the east of the continental divide showing the EJMT alignment, alignment No. 5448, and the three cross-sections selected to perform a 2-dimensional slope stability analysis.

To better understand the effect of tunnel location on slope stability, the modeled twin tunnels were translated horizontally and vertically into the slope, as shown in Figure 5.3. As previously mentioned, Alignments No. 5448 and 4995 were used as point of reference for the analysis, i.e., these alignments were used to determine the effect of tunnel translation into the slope below the crown of the slope and at the toe of the slope.

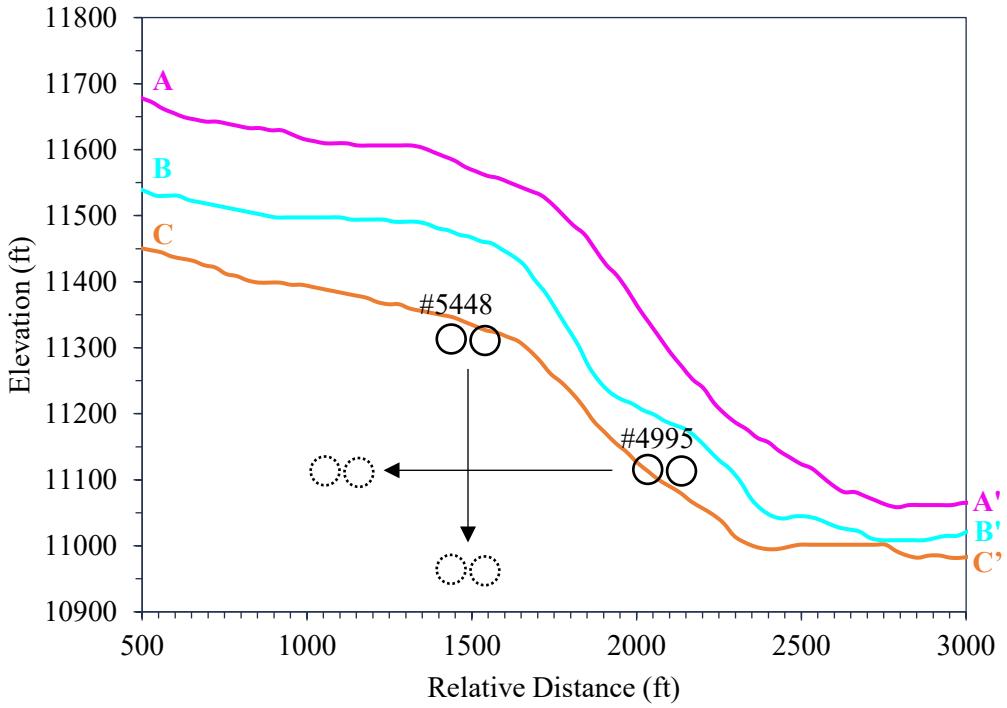

Figure 5.4: Cross-sections illustrating the approximate location of the proposed alignments No. 5448 and 4995 and their horizontal and vertical translation into the slope to determine the effect of tunnel location on slope stability.

5.3.2 Loveland Basin Landslide

The proposed alignments are relatively close to the Loveland Basin landslide, as shown in the plan view in Figure 5.4. Thus, a slope stability analysis of the Loveland Basin landslide was considered necessary to ensure the selected alignment will not cause the slide to reactivate.

The last slope stability analysis of the Loveland Basin landslide reported in the literature was performed by the Colorado Division of Highways (CDH) in 1971, using the Morgenstern and Price method. Their model considered two types of material properties: landslide and buttress fill. The material properties were based on engineering judgment rather than laboratory results, and groundwater level was not specified. The factor of safety obtained through their hand calculations resulted in an F=1.75 against deep movement (141-164 ft deep) and F=2.81 against shallow movement (98-125 ft deep). Based on these results, they recommended that the final volume of the buttress was at least 426,000 yd^3. A slope stability analysis was performed to verify these results using Slide2. Considering that the computational accessibility in 1971 was limited, the slope geometry was assumed to be a straight line with an average slope inclination of 27°.

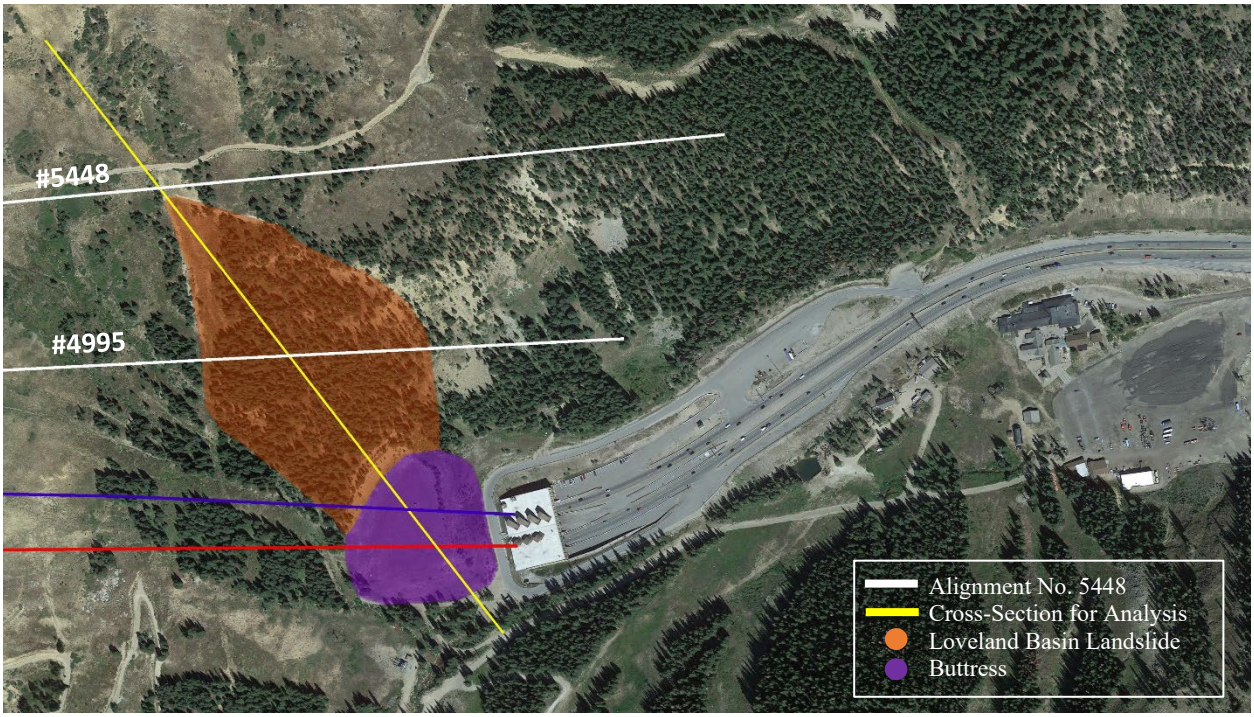

Figure 5.5: Plan view of the Loveland Basin landslide (orange area) and buttress (purple area) showing the EJMT alignment and the plausible location for the new tunnel bores (white lines).

To better represent the current conditions, additional 2-dimensional LE and FE models were developed considering a cross-section along the longest and deepest path of the landslide (see Figure 5.4). The actual soil profile was modeled using elevation data from Google Earth Pro, and the dimension and geometry of the slide were obtained from Lee & Mystkowski (1979), as shown in Figure 5.5. Specifically, a topographic map was overlayed with the isopach map to obtain the slide's thickness from top to bottom at every location of the selected cross-section. The surficial material was assumed negligible, and the rock mass was assumed to be ISF. A steel beam shield of about 16 inches thick was included in the model to simulate the support used in the existing tunnels.

Finally, the influence of the new tunnel bores on the stability of the Loveland Basin landslide was tested using a finite element model developed in RS2, shown in Figure 5.5. The new tunnels were assumed to have a circular shape with a radius of 27 ft. and a reinforced concrete liner of approximately 1 ft thick and separated at 118 ft. from center to center.

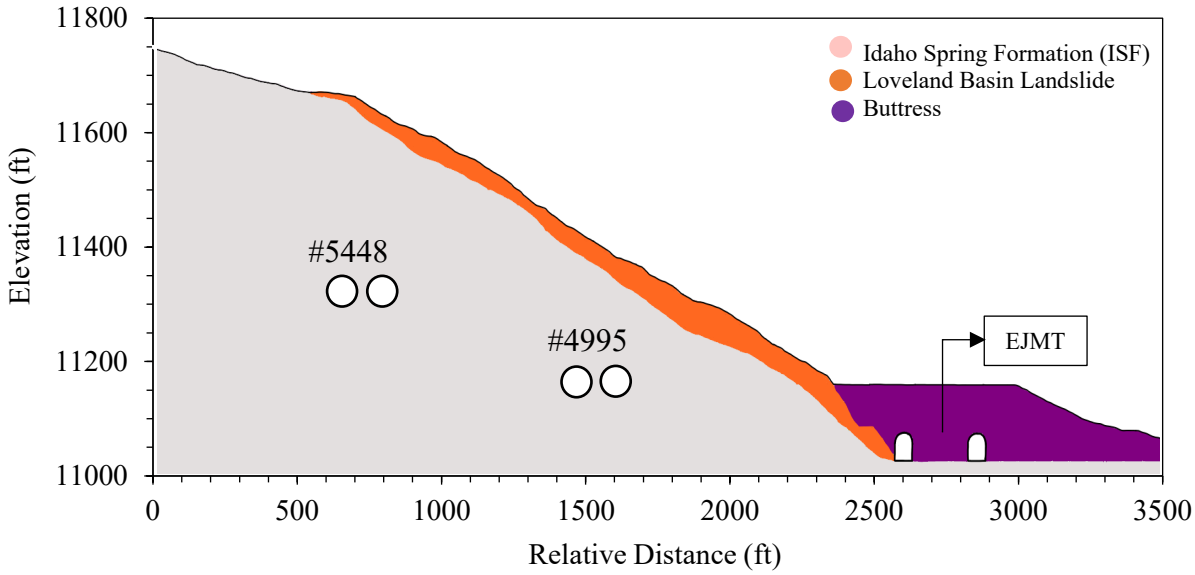

Figure 5.6: Finite element model of the Loveland Basin landslide showing the EJMT and the plausible location of the new tunnel bores relative to the landslide.

5.3.3 East Access Road

The east portal of alignment No. 5448 would be located approximately 304 ft. above the current elevation of I-70, at the entrance of the existing tunnels. This elevation difference could be covered in a distance of about 3 miles, resulting in a highway grade of approximately 6.6 %, slightly higher than the current approximation grade to the EJMT of 6%.

A similar right-of-way to the current I-70 was assumed to determine the slope cut. No detailed geometry was considered since it is out of the scope of this research. However, roadway geometry requirements are codified in the CDOT Roadway Design Guide. No fill was included at this stage due to the lack of compaction information and geomechanical properties of the material. Based on the OSHA safety guidelines, the slope cut was assumed as a single, 1:1 cut with no benching.

Seven cross-sections were analyzed to determine the factor of safety at different locations within the 3 miles radius mentioned above. No sensitivity analysis was carried out since this was only a complementary study related to the selection of alignment No. 5448.

5.4 Slopes West of the Continental Divide

The assumed coordinates for the west portal were 39° 40.814'N, 105° 56.068'W at an elevation of 11,216 ft, i.e., 42 ft. higher than the current west portal. The location of the west portal was shifted 500 ft west from the location proposed by Alexander (2022) to minimize the excavation efforts for the construction of an approximation road.

The slope geometry at the west portal was inconsistent, and the alignment of the new and existing tunnels described a relative angular position to the slope face. Thus, a 3-dimensional approach was considered adequate. Considering that the west side is not expected to show significant stability issues because the bedrock is predominantly comprised of competent granite, the model was simplified as a straight-line slope with an average angle of 30°, as shown in Figure 5.7.

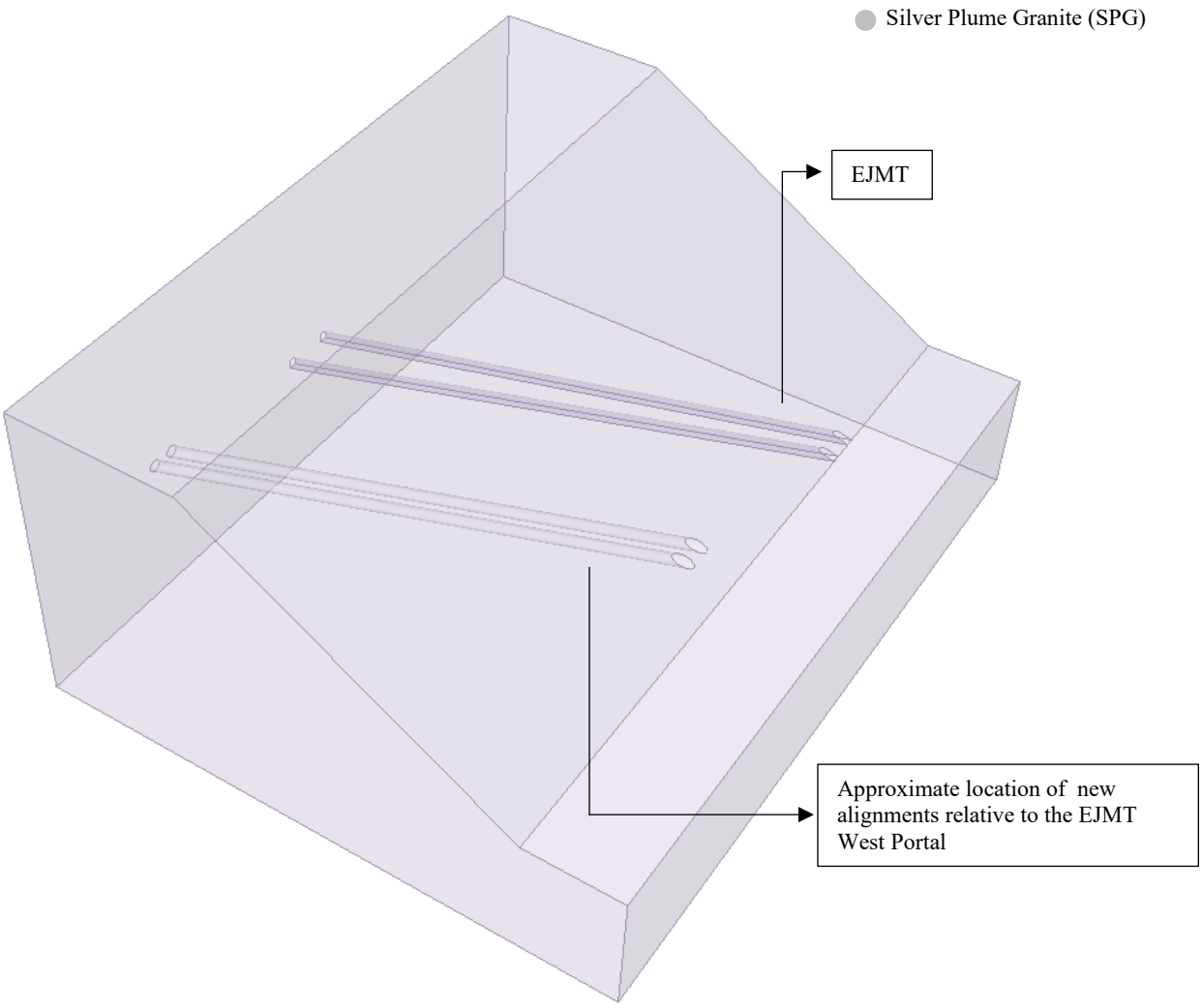

Figure 5.7: RS3 three-dimensional model used to analyze the slope stability at the new west portal location.

CHAPTER 6:
DETERMINISTIC AND PROBABILISTIC SLOPE STABILITY ANALYSIS TO EVALUATE TUNNEL LOCATION

6.1 Slope Stability Analysis of the Loveland Basin Landslide

The first analysis of the Loveland Basin landslide was intended to replicate the model developed by the CDH in 1971. The results obtained from Slide2 showed a relatively good agreement to the safety factor against deep movement with an average value of F = 1.60 for slip surfaces ranging from 141 ft. to 192 ft. at the deepest point. These results correspond to an 8.7% below the value reported by the CDH. On the other hand, the average safety factor for slip surfaces ranging from 1 ft. to 137 ft. at the deepest point was F = 1.40, i.e., approximately 50 % below the value reported by the CDH. No records of the modeling assumptions considered by the CDH were found during the literature review. Thus, it is difficult, if not impossible, to determine the reason for such a significant difference in the safety factor against shallow movement. Possible explanations could involve the use of a different cross-section, simplifications of the slope geometry, or the use of a single material type to model the slope.

For consistency, the second analysis of the Loveland Basin landslide was developed in Slide2 using the Morgenstern and Price method. The slide was modeled using the actual slope profile, the slip surface depth was based on geophysical estimations, and the landslide material was overlaid the ISF rock mass. The factor of safety without limiting the slip surface's entry or exit resulted in a value of F = 1.30.

Contrarily to the circular failure surface assumed in LE methods, the failure mechanism obtained from the FE model seemed to show translational features, as shown in Figure 6.1. Furthermore, sliding was entirely located on the landslide material (shallow movement), where total displacement larger than 1.5 ft. was found up to 18 ft. deep. The maximum total displacement was approximately 12 ft between 11,496 ft and 11,549 ft. The strength reduction factor resulted in a value of SRF = 1.25, about 3.84 % below the factor of safety obtained from Slide2 for shallow movement.

The results from the finite element model, including the excavation of the two new bores, resulted in an SRF = 1.19, i.e., 4.80% below the SRF without excavation. The location and type of failure were similar, but the maximum displacement decreased to 9.5 ft. Therefore, failure is possible but unlikely to occur under the current conditions, and the presence of the new tunnel bores might increase the instability of the Loveland Basin landslide, causing a shallow, translational landslide.

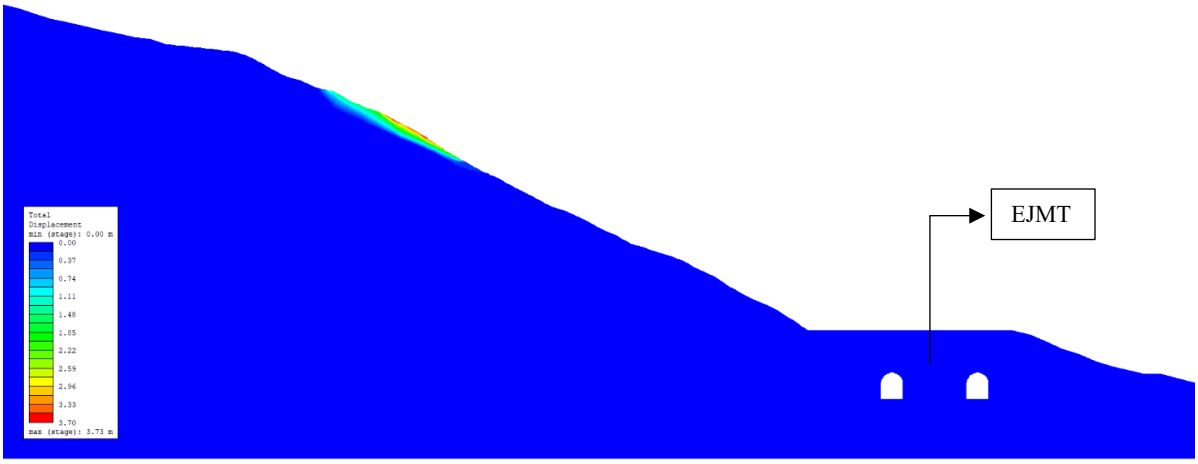

Figure 6.1: Total displacement result obtained from a finite element analysis of the Loveland Basin landslide.

It is worth noting that failure was originated in an area where the slope angle was slightly higher than the assumed internal friction angle of the landslide material, i.e., $\emptyset' = 34°$. However, wooden and non-wooden vegetation on top of the landslide might add some degree of cohesion to the topsoil and reduce surficial movement. Another RS2 model was developed, assigning a random cohesion value of $c' = 0.03$ MPa to the landslide material, resulting in a strength reduction factor of SRF = 1.68 and a maximum total displacement of only 1.45 inches. It is of the opinion of the author that these results more accurately represent the real conditions of the Loveland Basin landslide based on visual observations.

6.2 Effect of Tunnel Location on the Slope Stability – East Portal

The strength reduction factors obtained from each simulation, SRF, were normalized against the strength reduction factor for the slope before excavating the tunnels, SRF_0. Additionally, the horizontal and vertical translations were normalized against the diameter of the tunnel bores, D. Notice that the translation ratio increased as the tunnel bores were moved into the slope.

Based on a universe of 702 simulations, it was observed that the effect of tunnel location on slope stability has a distinct behavior, regardless of parameters such as slope geometry, material properties, groundwater table, and snow loads. In general, the horizontal translation of twin, circular tunnels to a distance x = 1.5D from the slope face resulted in an average reduction of the slope stability of approximately 30%, relative to the slope without excavations. Furthermore, the influence of tunnel location on the SRF value was minimal for a distance of approximately x = 5.5D, as shown in Figure 6.2. On the other hand, the vertical translation of the twin tunnels showed little to no overall effect on the slope stability, as shown in Figure 6.3.

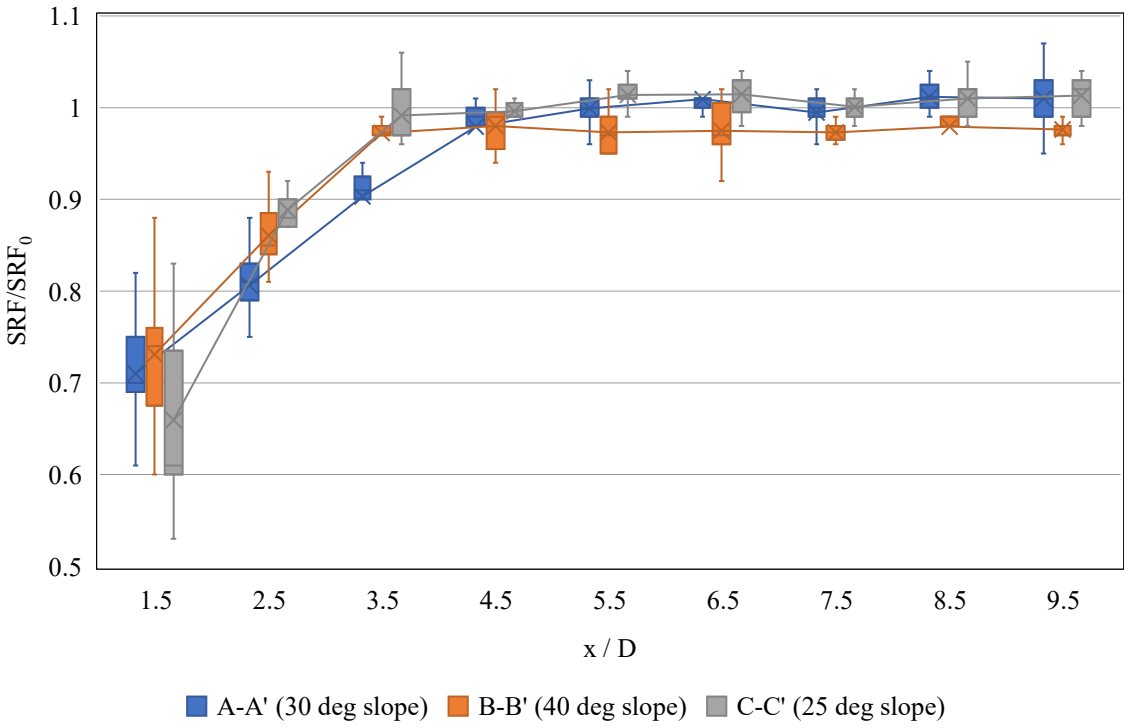

Figure 6.2: Effect of horizontal translation of twin tunnels on slope stability for varied slopes and material properties.

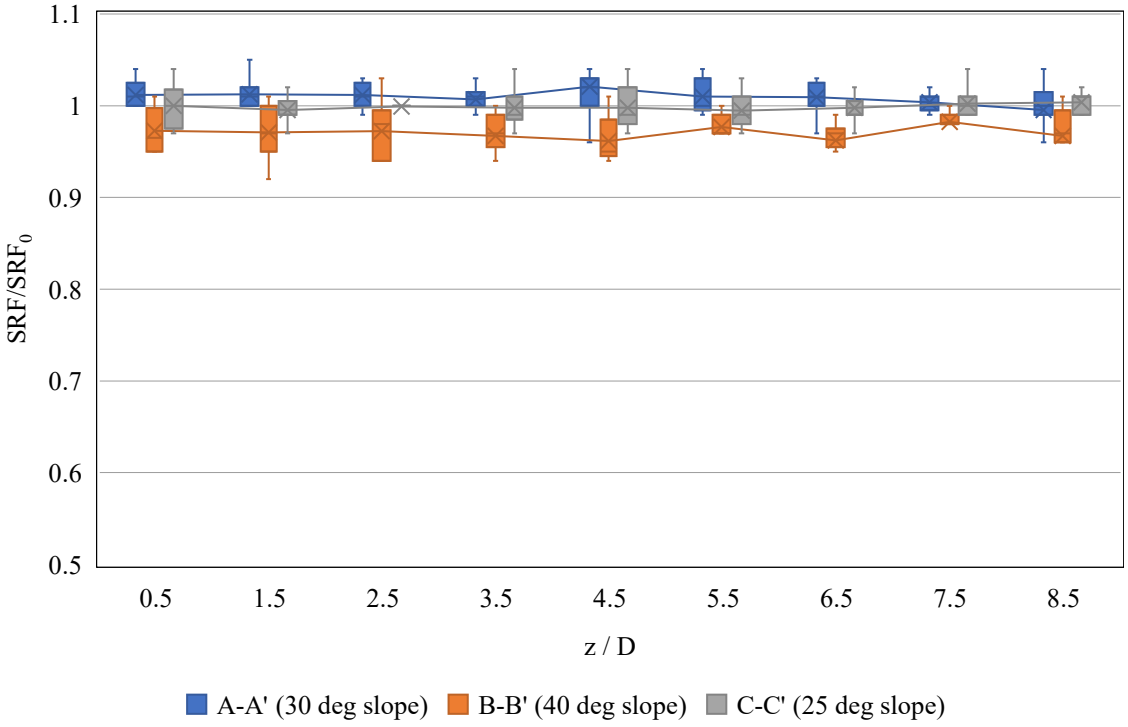

Figure 6.3: Effect of vertical translation of twin tunnels on slope stability for varied slopes and material properties.

This behavior was believed to be related to the relative location of the twin tunnels to the maximum shear strain contours found in the models, which indicated where the maximum plastic deformation was occurring, i.e., the possible location of the failure surface. For most cross-sections analyzed, the failure surface appeared to start nearby the crest of the slope, approximately 1500 ft south of the highest point, and exit at the lowest point right before I-70 (refer to Figure 5.6, pg. 43). When the horizontal translation of the twin tunnels was x = 5.5D or less, the failure surface seemed to be shifted directly through the tunnel openings resulting in a significant reduction of the SRF value. Contrarily, the proposed location of the additional twin tunnels was below the crest or further into the slope. Hence, the vertical translation to higher depths increased the distance between the openings and the maximum shear strain contour, resulting in minimal slope stability changes.

These results suggest that the additional EJMT tunnels should be located at least x = 5.5D into the slope. However, under certain circumstances, this critical distance might not be achievable. For instance, if the slope strike and the tunnel alignment are not perpendicular, there will be an area where the tunnel entrance is closer than 5.5D to the slope face. Furthermore, the SRF values showed considerable uncertainty at distances less than 3.5D. Thus, the effect of each variable on the SRF for a horizontal translation of the tunnels was studied. Since no significant variations of the SRF were observed for a vertical translation for other variables, the analysis was focused on the horizontal translation of twin tunnels.

6.2.1 Effect of Slope Geometry

Variations in the shape of the base models were considered to account for the uncertainty of digital surveying. Specifically, the shape of the slopes was simplified as straight-line slopes with slope angles equal to the average inclination obtained from the base models, i.e., 30º, 40º, and 25º for cross-sections A-A', B-B', and C-C', respectively. For this particular sensitivity analysis, the SRF was normalized against the strength reduction factor obtained for the original slopes. The results for horizontal translation are shown in Figure 6.4.

From Figure 6.4, it was observed that twin tunnels located at a horizontal distance of 1.5D from the slope face resulted in a reduction in the slope stability between 25 and 40%, based on the slope angle. The normalized SRF increased linearly with distance until convergence was achieved at approximately 3.5 – 4D. Based on the box and whiskers, it can be inferred that the SRF values for different slope shapes had minimal statistical dispersion, i.e., the shape of the slope had little to no effect on slope stability.

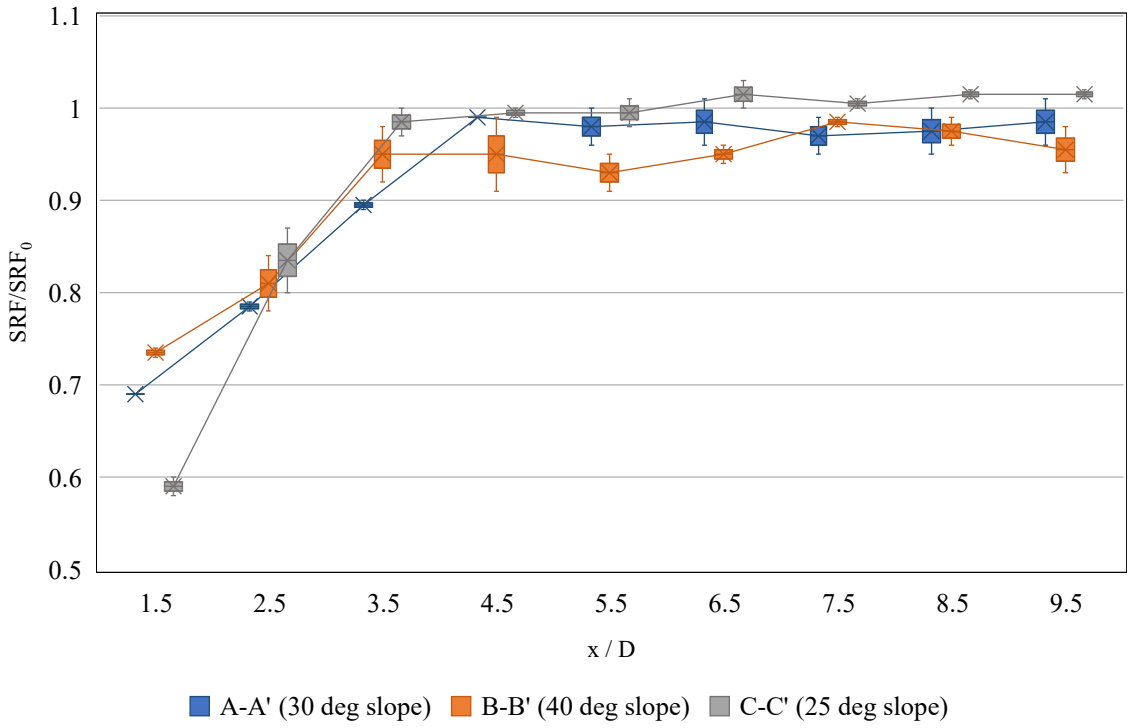

Figure 6.4: Plot showing the normalized SRF versus the normalized horizontal translation of twin, circular tunnels into the slope.

6.2.2 Effect of Material Properties

Typically, the reported mechanical properties of a rock mass are highly variable. Although unfavorable for computational simulations, it is impractical and excessively costly to drill a sufficiently large number of boreholes to perform laboratory samples and obtain reliable data. Thus, approximations and engineering judgment is usually used by geotechnical engineers.

The material properties at the location of interest have been extensively documented (refer to section 2.5). However, it is possible and probable to encounter variations in their values at different site locations. Therefore, a sensitivity analysis was performed to determine the effect of the friction angle and cohesion of the ISF on slope stability, as shown in Figures 6.5 and 6.6, respectively. Specifically, friction angle was modified from -35% to +20%, and cohesion was modified between -35% and +35% of the values reported in Table 2.2.

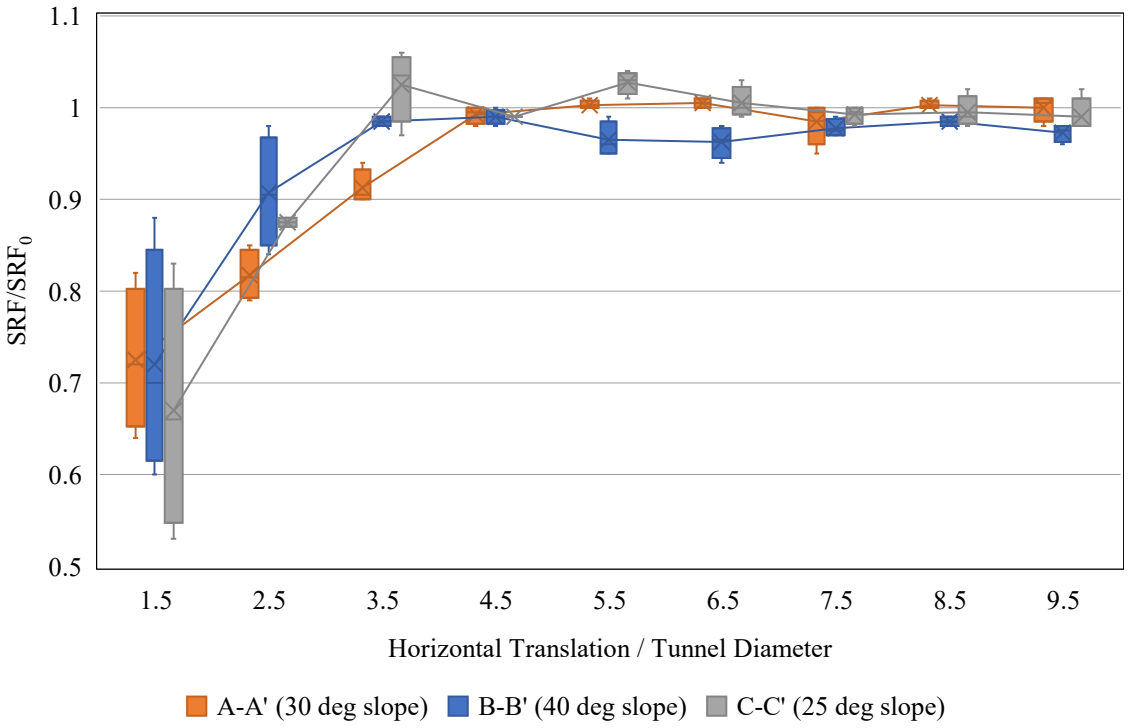

Figure 6.5: Plot showing the normalized SRF vs. the variation of friction angle for different slopes.

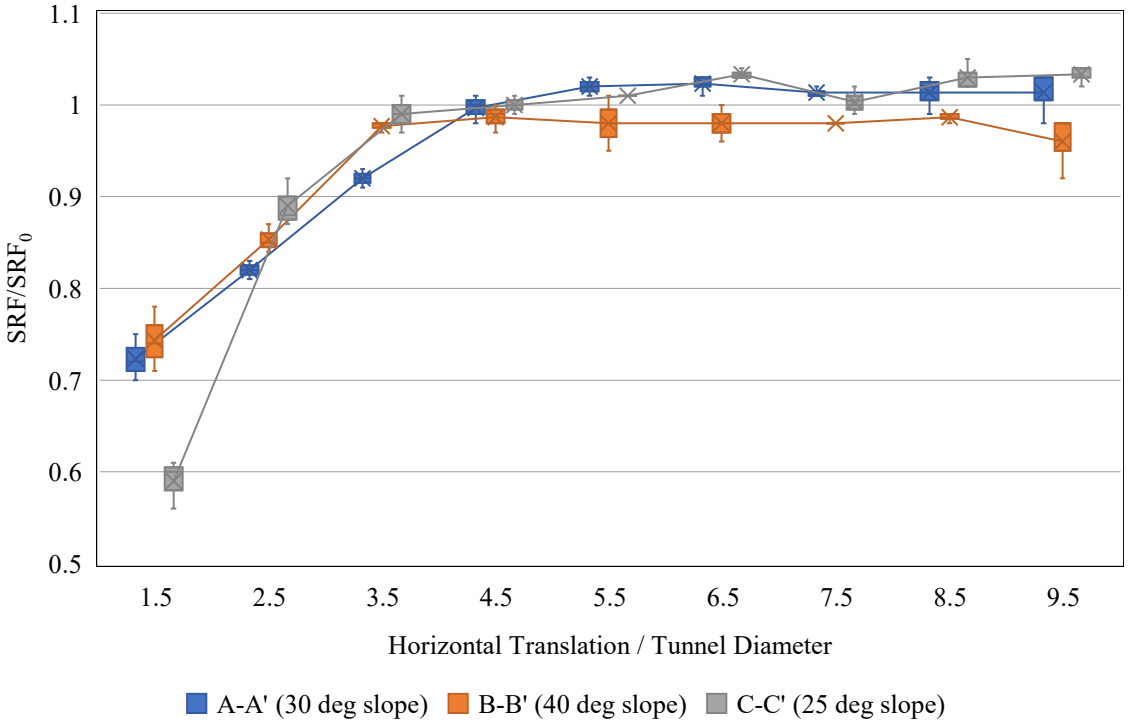

Figure 6.6: Plot showing the normalized SRF vs. the variation of cohesion for different slopes.

From Figure 6.5, it was observed that the location of twin tunnels at a horizontal distance of 1.5D from the slope face resulted in an average slope stability reduction of approximately 30%. The normalized SRF increased logarithmically with distance until convergence was achieved at approximately 4.5 – 5D. According to the significant statistical dispersion of the SRF values for distances less than 3D, it can be inferred that the friction angle is a critical parameter in slope stability. For instance, when the twin tunnels were about 1.5D from the slope face, the variation on the SRF ranged approximately ±25%.

Figure 6.6 shows that the SRF for slopes with varied cohesion decreased by 40% when tunnels were located at 1.5D from the slope face on a 25-degree slope. Like the previous scenario, the normalized SRF increased logarithmically with distance until convergence was achieved at approximately 4.5D. The compact box size and the limited whisker length of all distances evaluated suggest that cohesion had little effect on slope stability. In particular, the maximum variation on the SRF was approximately ±5% at a distance of 1.5D on a 40-degree angle.

6.2.3 Effect of Groundwater Depth

The groundwater table at the location selected for the new east portal has not been documented. However, field investigation performed in the area in the last decades suggested that the depth of the water table might range from about 16 ft to 82 ft. Water in the area is highly dependent on seasonal availability from snowpack melting. Thus, to account for the uncertainty of water levels, three different scenarios were tested: fully submerged slope, GWT at 50 ft, and GWT at 85 ft. The results are shown in Figure 6.7.

From Figure 6.7, it can be observed that the location of twin tunnels at a horizontal distance of 1.5D from the slope face results in an average slope stability reduction of approximately 30%. The normalized SRF increased logarithmically with distance until convergence was achieved approximately at 5 – 5.5D. Due to the significant statistical dispersion of the SRF values at all distances, it was confirmed that the depth of the groundwater table is a critical parameter to consider for slope stability analysis. Uncertainty was notably high when tunnels were located at distances less than 3D. For instance, when the twin tunnels were at 1.5D from the slope face, the variation on the SRF ranged approximately ±25%.

Considering the significant effect of the location on the groundwater table on the stability of the slopes, it is paromount to perform field measurements of this input parameter to obtain the actual factor of safety of the slope. Furthermore, if failure occurs above the groundwater table, unsaturated soil mechanics theories should be incorporated into the analysis.

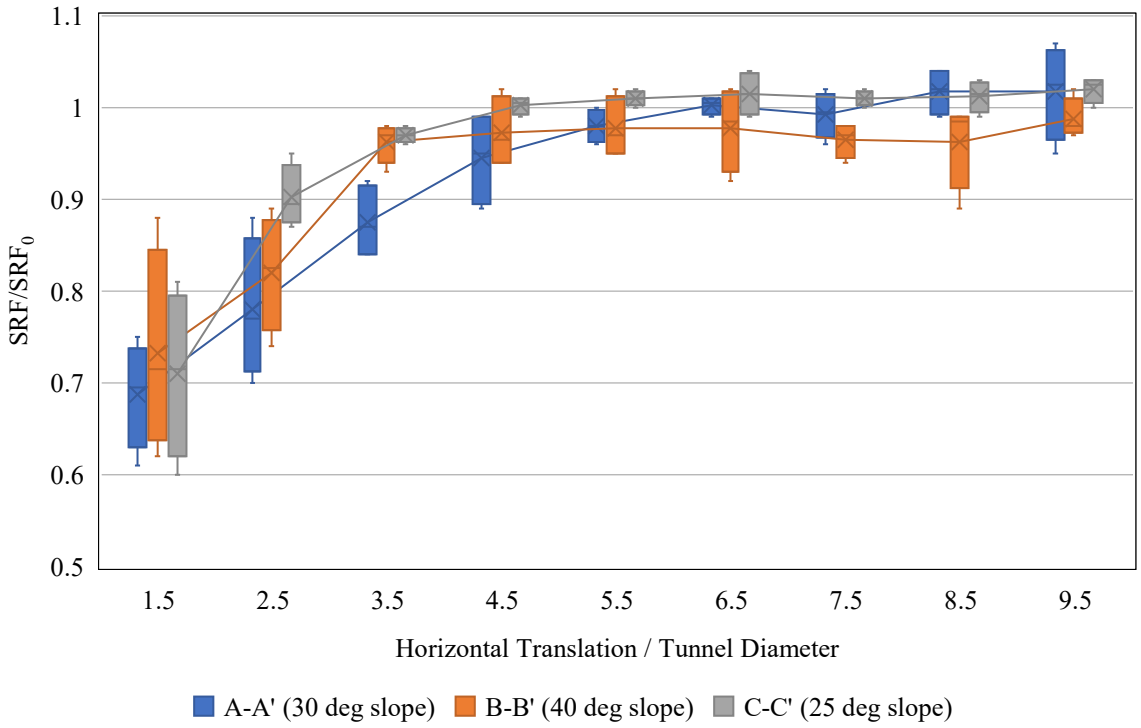

Figure 6.7: Plot showing the normalized SRF at different tunnel locations for varied depths to the groundwater table.

6.2.4 Effect of Snow Loads

Snow loads are usually not considered in slope stability analysis, probably because mountainous terrains at a high elevation, such as the Rocky Mountains, are rare in most parts of the United States. In the vicinity of the EJMT, snow accumulation can be as much as 10 ft, and the frozen layer can be as thick as 2.5 ft. Therefore, a sensitivity analysis was performed to determine the effect of snow loading on slope stability, as shown in Figure 6.8.

Figure 6.8 showed that the stability of slopes rapidly declined as the twin tunnels were closer to the slope face, especially for shallower slopes. For instance, when the tunnels were at 1.5D from the slope face on a 25-degree slope, the SRF decreased by approximately 35%. Following the same trend as in previous cases, the normalized SRF increased logarithmically with distance until convergence was achieved at approximately 4.5D. The compact box size and the limited whisker length observed at all locations suggested that external loading had little effect on slope stability. In particular, the maximum variation on the SRF was approximately ±2.5% when the tunnels were located at 1.5D on the 25-degree angle.

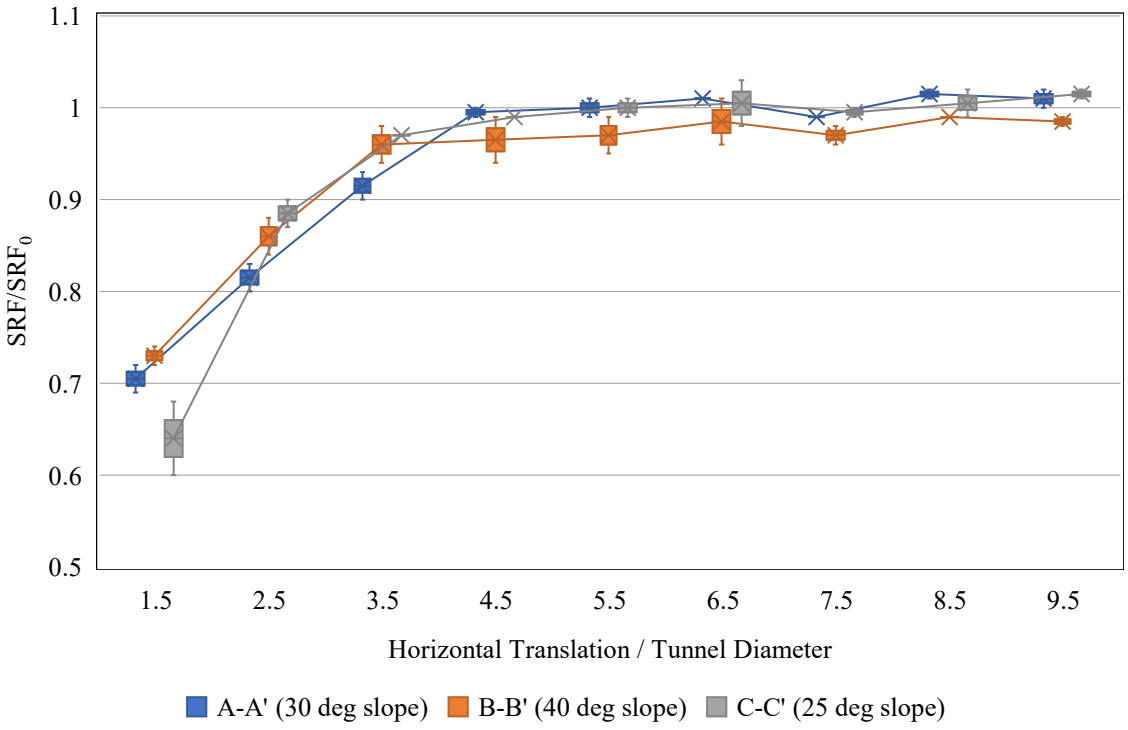

Figure 6.8: Plot showing the normalized SRF at different tunnel locations, including snow loads.

6.2.5 Probabilistic Slope Stability Analysis

Spatial variability of material properties, limited field investigations, lack of reliable data, changing environmental conditions, or simply complex ground conditions are some factors causing high uncertainty of geotechnical simulations.

RS2 offers probabilistic analysis capabilities to determine the effect of uncertainty of input parameters through Monte-Carlo simulations. However, they are limited to analyzing the uncertainty of material properties such as cohesion or friction angle. For the current study, several other parameters were evaluated besides material properties, namely, slope geometry, groundwater level, and snow loads. Thus, "manual" analysis was the preferred method to determine the probability of failure, P_f, for the slopes in the vicinity of the new east portal when the value of SRF <1. Although this methodology does not fall within the traditional probabilistic analyses, the results from the current probabilistic analysis provided a general idea of the behavior at the research site. Advanced methods should be used to validate the proposed values and provide more robust results regarding the probability of failure of the slopes in the vicinity of the EJMT.

The probabilistic analysis used approximately 33 values of SRF for each tunnel location for a total of 594 simulations. The skewness for all distributions analyzed, i.e., the asymmetry of the distribution

around the mean, showed to be reasonably low. Thus, a normal distribution seemed an adequate choice to characterize the strength reduction factors. For reference, the distribution for twin tunnels located at a horizontal distance of 5.5D from the slope face is shown in Figure 6.9.

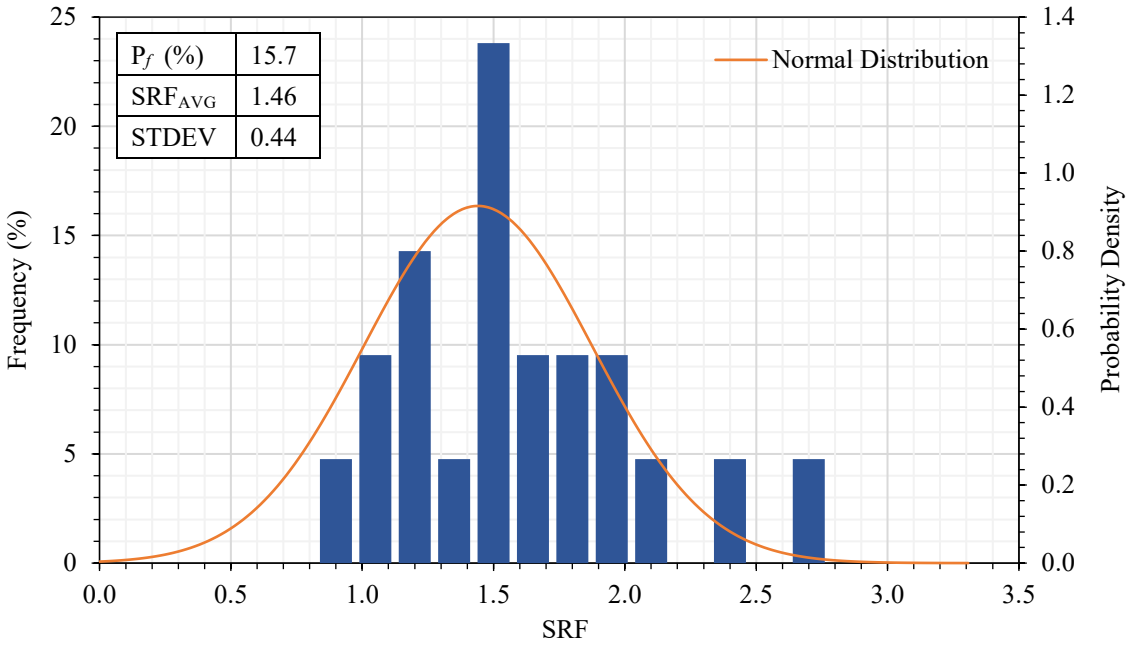

Figure 6.9: Strength reduction factor histogram and normal probability function for a horizontal translation of x = 5.5D considering a variety of slope geometry and material properties.

The slopes in the vicinity of the possible east portal area showed to be highly sensitive to the horizontal translation of twin tunnels, as shown in Figure 6.10. The average factors of safety obtained at several different horizontal distances showed to be greater than one, except for twin tunnels located at 1.5D from the slope face into the slope. These results implied that the slopes are "safe" based on the deterministic approach. However, the probability of failure reached values as high as $P_f = 0.66$ when the tunnel location was 1.5D. From Figure 6.10, it can be observed that independently of the slope geometry, material properties, groundwater table, and external loads applied to the slope, the tunnel-slope interaction is minimized at a horizontal distance of 5.5D. In other words, tunnels beyond this critical section could be assumed to be as stable as the slope without tunnels.

On the other hand, the vertical translation of twin tunnels showed little to no influence on either the factor of safety or the probability of failure, as shown in Figure 6.11. In general, the factor of safety and the probability of failure showed relatively constant for all cases analyzed. Although this is not good in terms of tunnel location optimization, it suggests that the slope after the construction of twin tunnels will be as stable as the slope without the tunnels.

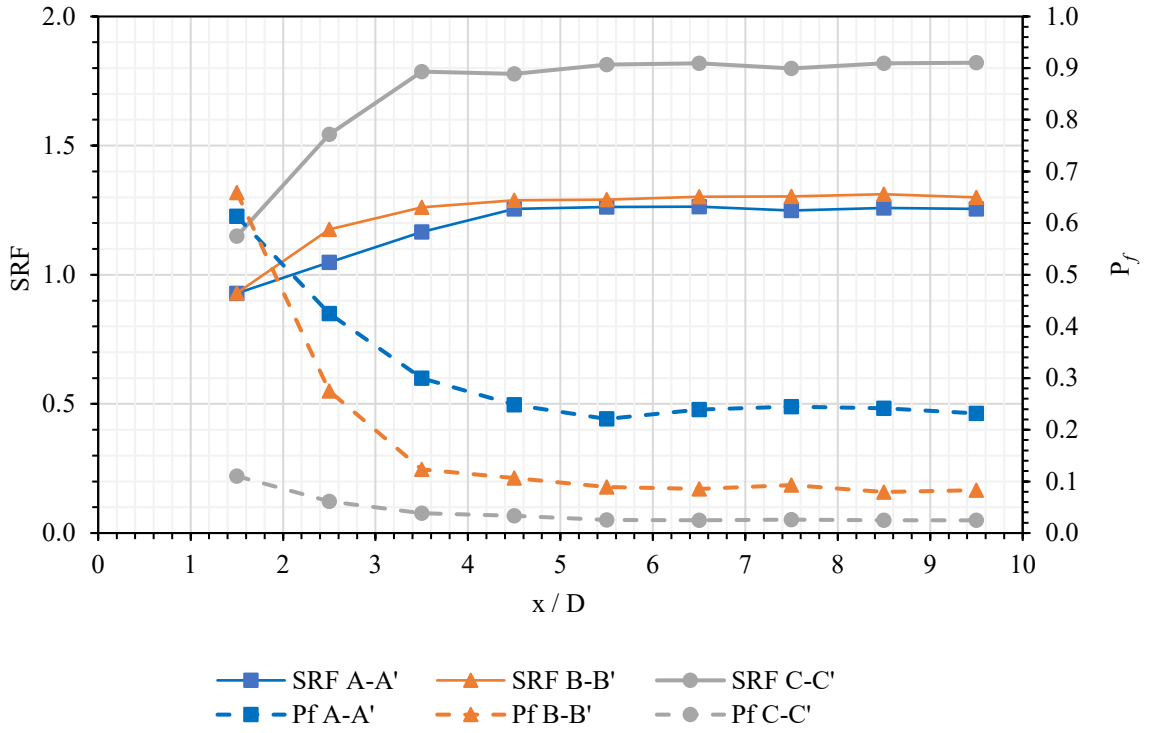

Figure 6.10: Plot comparing the probability of failure for a horizontal translation of twin tunnels into the slope versus the strength reduction factor.

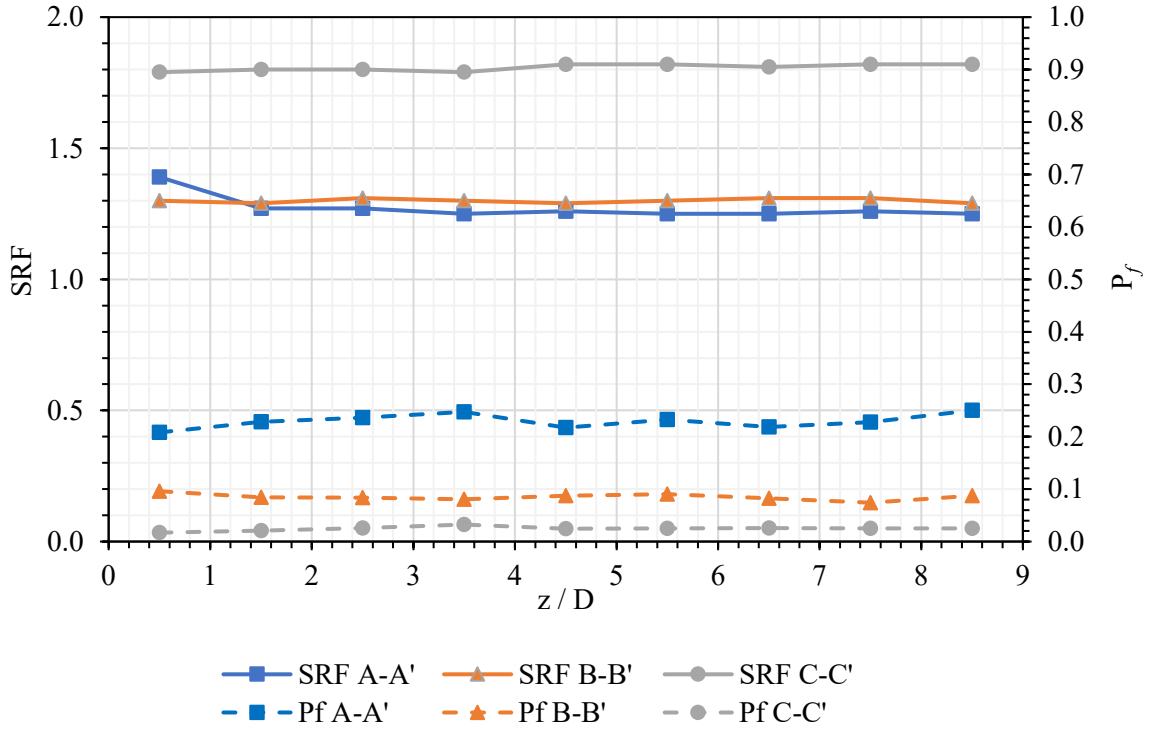

Figure 6.11: Plot comparing the probability of failure for a vertical translation of twin tunnels into the slope versus the strength reduction factor.

According to Duzgun, Yucemen, & Karpuz (2003), "acceptable" values of probability of failure for rock slopes range between 0.10 and 0.15. Similarly, USBR-USACE (2015) indicated that failure is unlikely to occur when $P_f \leq 0.1$. Using the USBR-USACE threshold for unlikely failure and the best-fit curve shown in Figure 6.12, the factor of safety obtained for a $P_f \leq 0.1$ was approximately SRF = 1.4. This value of 1.4 is very close to 1.5 as the minimum accepted factor of safety for judging potential slope failure in practice.

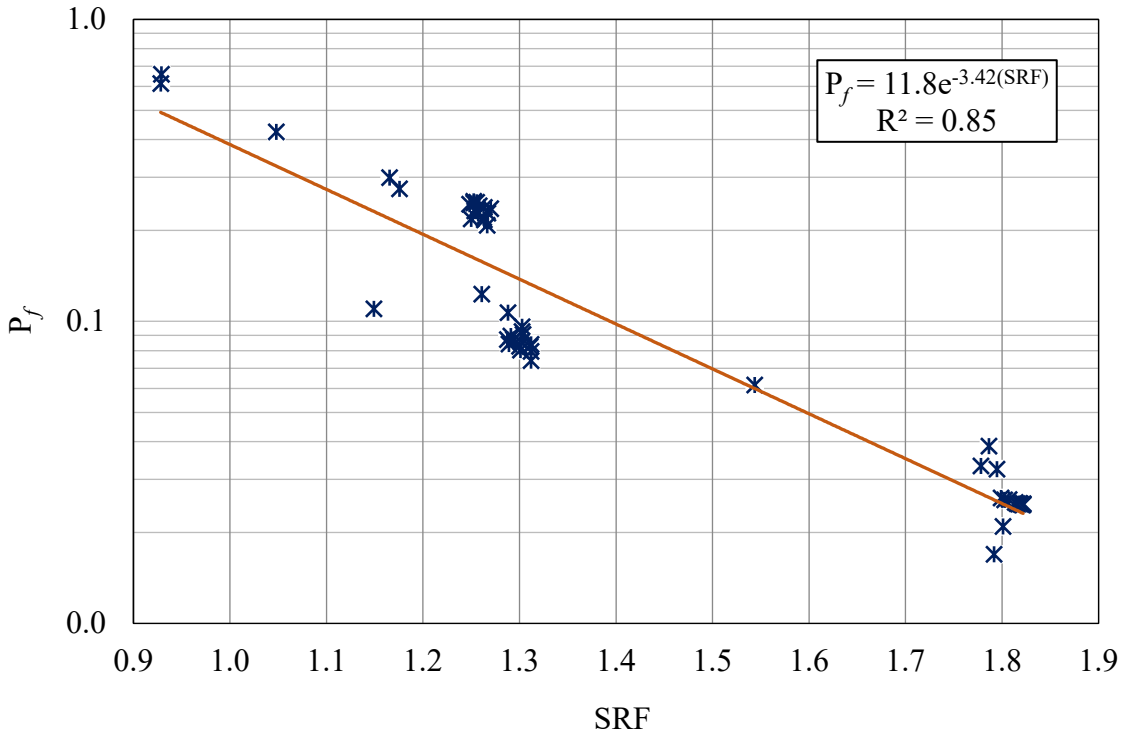

Figure 6.12: Probability of Failure (in log scale) versus the Strength Reduction Factor (or Factor of Safety) for the slopes near the new EJMT east portal.

From the results presented in this section, it can be inferred that tunnels located at least 5.5D and 2.5D into the slope would be within acceptable values for cross-sections B-B' and C-C', respectively. However, cross-section A-A' (furthest from the entrance) showed the lowest factors of safety and highest probabilities of failure at almost every location analyzed for the twin tunnels. Furthermore, the probability of failure for cross-section A-A', despite the translation of the twin tunnels, resulted in a $P_f \geq 0.22$.

Data post-processing indicated that the standard deviation of SRF values for cross-section A-A' was 53.2% and 26.8% higher than those of cross-sections B-B' and C-C', respectively. As mentioned in Section 4.2.3, higher values of Vc result in larger probabilities of failure; however, it is unclear to the author if a direct comparison can be done between the dispersion of deterministic SRF values and the

coefficient of variation. If anything, these results suggest that cross-section A-A' has a higher sensitivity to changes in geometry, material properties, and groundwater level and that a detailed study should be performed to understand the failure mechanism at each location for the twin tunnels.

6.3 Effect of Tunnel Location on the Slope Stability – West Portal

Based on the literature (Richards, 1963; Mattei, 1965; Robinson, et al., 1974), the bedrock comprised competent granite to the west of the continental divide. Less faulting and weathering have been mapped, and slope stability is expected to be substantially higher than at the east portal. Additionally, the slope geometry was relatively consistent throughout the slope; hence an average slope angle was assumed for the slope stability analysis.

The 3-dimensional finite element simulation for the current conditions resulted in an SRF = 5.55, and after excavating the twin tunnels, the SRF decreased by 35.5% to a value of SRF = 3.58. Tough the stability of the slope showed a significant reduction due to the excavation of the new tunnels, the maximum total displacement was only 2.3 inches (0.058 m) at the center of the slope, as shown in Figure 6.13.

A sensitivity analysis of some critical parameters considered in the Generalized Hoek-Brown resulted in a reduction of the SRF of approximately 21.8% and 17.3%, for a drop of 50% of the values reported in Table 2 for the GSI and UCS, respectively.

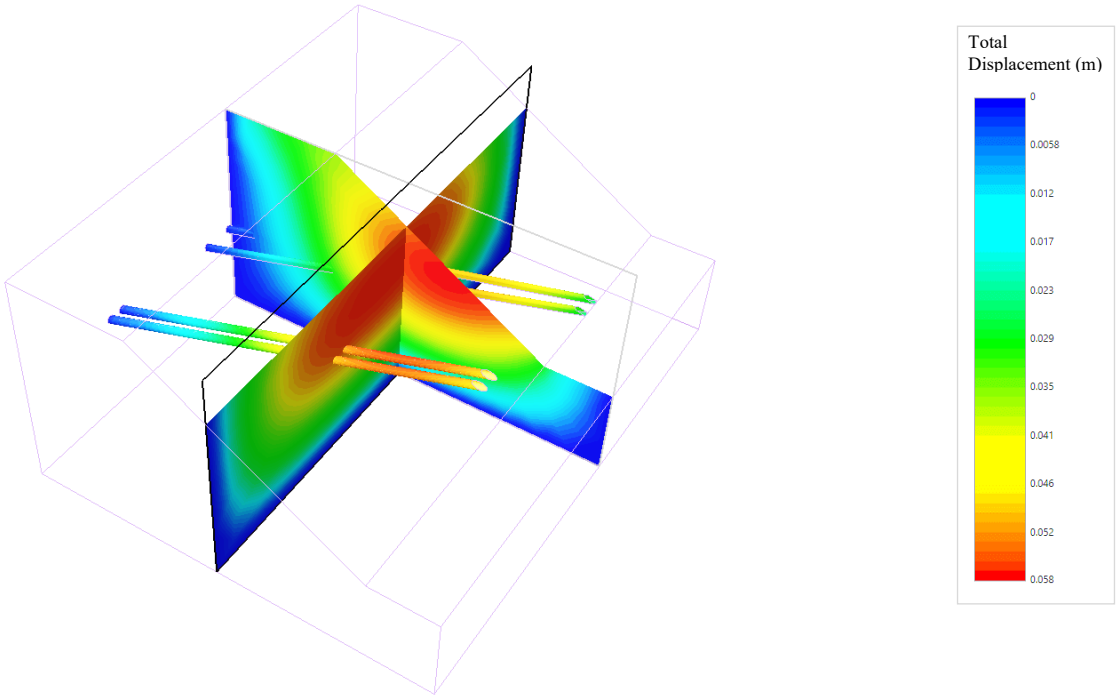

Figure 6.13: Result for total displacement obtained from a 3-dimensional finite element analysis after excavating twin tunnels in the vicinity of the EJMT.

6.4 Effect of Slope Cut on Slope Stability

Seven cross-sections along the 3-mile-long access road were used to determine the stability of slopes west of the new tunnel portal. Similar to the analysis of cross-sections A-A', B-B', and C-C', the bedrock was assumed to be ISF, and no groundwater and snow loads were included in the model. Furthermore, the slope cut was assumed to be identical for all cross-sections regardless of the height, i.e., a horizontal cut of approximately 130 ft into the slope and a 1:1 slope ratio, as shown in Figure 6.14. Based on all these assumptions, the sole factor affecting the results was the slope geometry, as shown in Figure 6.15.

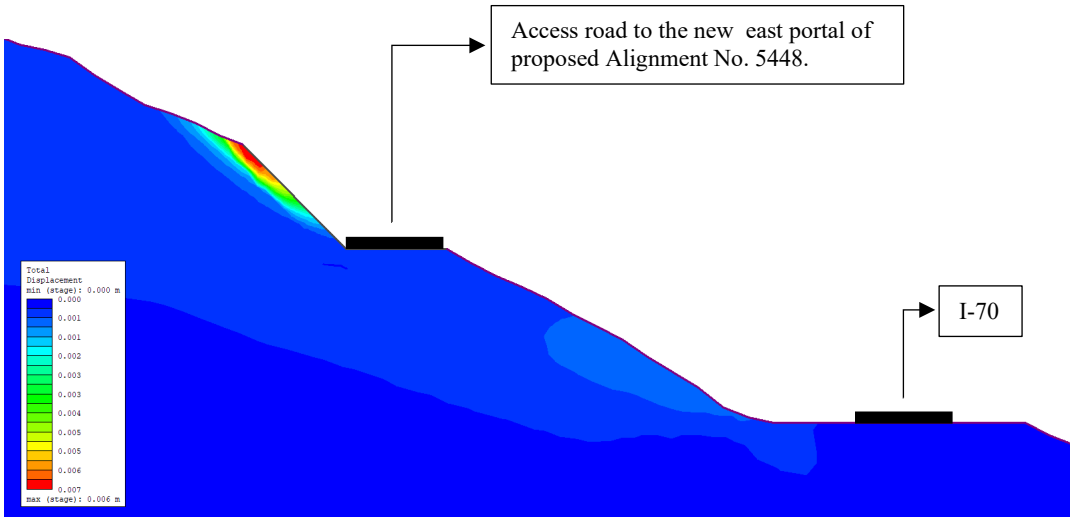

Figure 6.14: Typical result for total displacement obtained from a 2-dimensional finite element analysis.

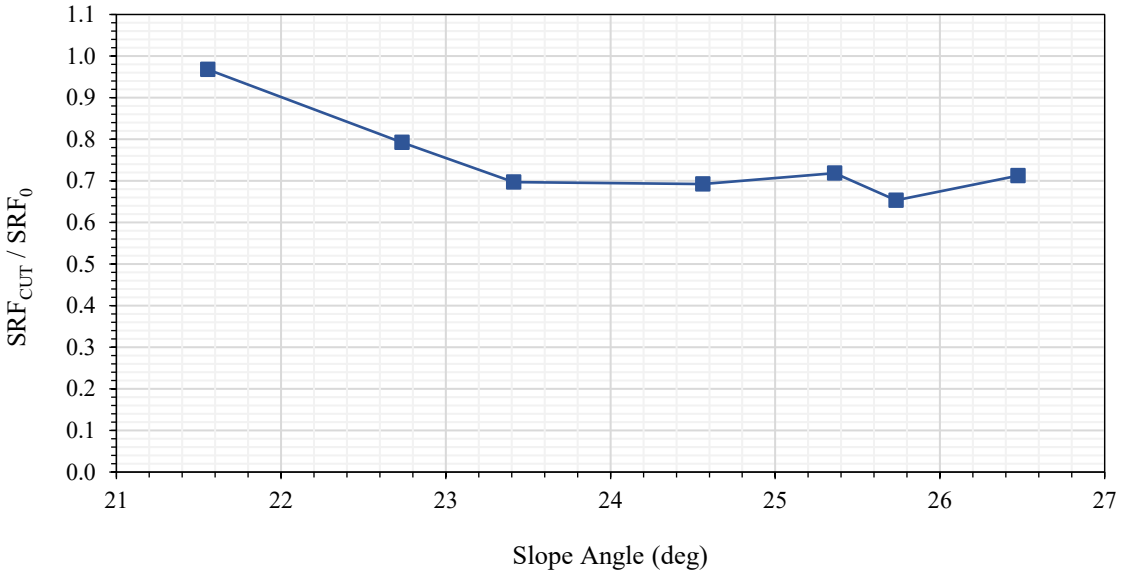

Figure 6.15: Plot showing the effect of slope angle on the SRF values after the excavation of a slope cut.

Figure 6.14 shows that failure due to a basic slope cut on the slopes to the east of the new east portal occurred at the crown of the cut and showed translational features. The maximum total displacement for all cross-sections resulted in less than an inch, i.e., negligible sliding. Furthermore, since no signs of a deep-seated failure were observed, the author believes that benching, shotcrete, or nailing would be sufficient mitigation measures to prevent material from sliding onto the access road.

From Figure 6.15, it can be observed that the slope geometry significantly influences the strength reduction factor after the excavation of a slope cut. For instance, an increase of only 5 degrees on the slope angle reduced the SRF by approximately 30%. These results align with the results obtained in section 6.2.1 after convergence, i.e., the increase in slope angle caused a reduction in slope stability.

CHAPTER 7:
CONCLUSIONS & RECOMMENDATIONS

7.1 Conclusions

This report has finished performing a deterministic and probabilistic slope stability analysis of the area where potential tunnel portals might be located during the expansion of the new tunnel bores of the Eisenhower-Johnson Memorial Tunnels. According to the information collected, it can be concluded that:

1. The slope stability analysis for the current conditions of the Loveland Basin landslide resulted in an FS = 1.3 and SRF = 1.25 using LE and FE methods, respectively. The addition of the selected tunnel location into the model caused a reduction in the factor of safety of the Loveland Basin landslide of approximately 4.8% relative to current conditions, i.e., SRF = 1.19.
2. The stability of the slopes east of the continental divide was highly sensitive to slope geometry, friction angle, and depth to the groundwater table. Contrarily, cohesion and external loads did not cause significant changes in the overall slope stability.
3. The slope west of the continental divide showed some sensitivity to variables such as the GSI and UCS. Despite the radical reduction in strength parameters, the slope appeared to be stable and minimal displacement was obtained due to the addition of twin bores into the model.
4. Slope stability increased as tunnel bores were translated into the slope to higher overburden areas. Horizontal translation of twin tunnels showed an average reduction in the factor of safety of up to about 30% and an increase in the probability of failure of about 37% when the twin tunnels were located at a distance of x =5.5D or less from the slope face. Vertical translation of the proposed twin tunnels showed little to no effect on the overall behavior of the slope.
5. The inherent probability of failure of the slope east of the continental divide was P_f = 14.6%, regardless of changes in slope geometry, material properties, groundwater level, and external loads. Although the deterministic analysis showed that most simulations have an SRF > 1, i.e., safe, there is still a probability that the slopes could fail.
6. Deep movement and structurally controlled failure are unlikely to occur in the research area.
7. Limited stability issues or movement were observed in the simulations due to the slope cuts for the construction of the access road to the new east portal.

Based on the results and conclusions, the author believes that alignment No. 5448, selected as the baseline for this study, provides enough clearance from the slope face to minimize the probability of failure. However, it is inevitable that alignments relatively perpendicular to the slope face do not reach a critical distance near the exits. Thus, careful consideration should be placed into the design of the portals.

7.2 Recommendations

Based on the limitations encountered during the realization of this paper, the following recommendations can be made:

1. Characterization of the rock mass strength of the ISF was limited due to the use of the M-C failure criteria. The geomechanical properties proposed in Table 2 and used as a baseline for the numerical simulations correspond to those of the intact material. Thus, lower factors of safety could be expected due to faults, joint blockiness, and weathering encountered in the research area. Although variations in the material properties were accounted for in the sensitivity analysis, the actual strength of the rock mass is uncertain. Further analysis of the rock mass strength is recommended to validate the results.
2. The numerical simulations assumed an isotropic and homogeneous material. While it was determined that structurally controlled failure is unlikely to occur in the research area, it might be recommendable to incorporate discontinuities in the models to account for structural geology, particularly on the slopes west of the continental divide.
3. The results obtained in this research are a function of the software used, i.e., Slide2, RS2, and RS3. It might be recommended to validate these results using other analysis methodologies such as discontinuum finite element modeling. This software would allow visualization of material detachment, which would be significantly valuable to determining potential rockfall avalanches.
4. Validation of proposed displacements was limited to visual observations during on-site visits. Field measurements would be highly recommendable to validate the results suggested in this document.

REFERENCES

Alexander, G. R. (2022). *Development of a Methodology for Probabilistic Alignment Slection and Design for Drill-and-Blast Hard-Rock Tunnels.* Golden, Colorado: Colorado School of Mines Thesis Repository.

Bishop, A. W. (1955). The Use of the Slip Circle in the Stability Analysis of Slopes . *Geotechnique Vol. 5 Issue 1*, 7-17.

Causse, L., Cojean, R., & Fleurisson, J.-A. (2015). Interaction between Tunnel and Unstable Slope - Influence of Time - Dependent Behavior of a Tunnel Excavation in a Deep-Seated Gravitational Slope Deformation. *Tunnelling and Underground Space Technology* , 270-281.

CDOT. (n.d.). *Eisenhower Tunnel Traffic Counts*. Retrieved from CDOT: https://www.codot.gov/travel/eisenhower-tunnel/trafficcounts

CDOTa. (2010). I-70 Mountain Corridor PEIS Geologic hazards technical report.

CDOTb. (2010). I-70 Mountain Corridor Revised Draft Programmmatic Environmental Impact Statement. *Project IM 0703-244*.

Duncan, J. M., Wright, S. G., & Brandon, T. L. (2014). *Soil Strength and Slope Stability.* Wiley.

Duncan, W. C., & Norman, N. I. (1996). Rock Slope Stability Analysis. *Landslides: Investigation and Mitigation*, 391-425.

Durgin, P. B. (1977). Landslides and the Weathering of Granitic Rocks. *Geological Society of America, Reviews in Engineering Geology, Vol. III*.

Duzgun, H., Yucemen, M., & Karpuz, C. (2002). A probabilistic model for the assessment of uncertainties in the. *Rock Mechanics and Mining Sciences 39*, 743-754.

Duzgun, H., Yucemen, M., & Karpuz, C. (2003). A Methodology for Reliability-Based Design of Rock Slopes. *Rock Mechanics and Rock Engineering 36 (2)*, 95-120.

Fell, R., Glastonbury, J., & Hunter, G. (2007). Rapid landslides: the importance of understanding mechanisms and rupture surface mechanics. *Quarterly Journal of Engineering Geology and Hydrogeology, 40*, (pp. 9-27).

Fell, R., Stapledon, D., & Macgregor, P. (2012). Landslides and Geologic Environments. *Landslides - Types, Mechanisms and Modeling*, 134-143.

Fellenius, W. (1936). Calculation of the stability of earth dams. *Transactions of the 2nd Congress on Large Dams Vol. 4* (pp. 445-462). International Commision on Large Dams of the World Power Conference.

Frohlich, O. K. (1953). The factor of safety with respect to sliding of a mass of soil along the arc of a logarithmic spiral. *Proceedings of the Third International Conference on Soil Mechanics and Foundation Engineering, Vol. 2*, (pp. 230-233). Switzerland.

Gattinoni, P., Consonni, M., Francani, V., Leonelli, G., & Lorenzo, C. (2019). Tunnelling in Landslide Areas Connected to Deep Seated Gravitational Deformations: An Example in central Alps (Northern Italy). *Tunnelling and Underground Space Technology 93*.

Gattinoni, P., Pizzarotti, E. M., & Scesi, L. (2014). *Engineering Geology for underground Works.* Springer.

Griffiths, D. V., & Fenton, G. A. (2004). Probabilistic Slope Stability Analysis by Finite Elements. *Journal of Geotechnical and Geoenvironmental Engineering, Vol. 130, No. 5*, 507-518.

Griffiths, D. V., & Lane, P. A. (1999). Slope Stability Analysis by Finite Elements. *Geotechnique 49, No. 3*, 387-403.

Harker, I. R. (1996). Curved Tree Trunks-Indicators of Soil Creep and Other Phenomenal . *The Journal of Geology, Vol. 104*, 351-358.

Hoek , E., Carranza-Torres, C., & Corkum, B. (2002). Hoek-Brown Failure Criterion – 2002 Edition. *Proceedings of the NARMS-TAC Conference*, (pp. 267-273). Toronto, Ontario.

Hoek, E., & Brown, E. (2019). The HoekeBrown failure criterion and GSI e 2018 edition. *Journal of Rock Mechanics and Geotechnical Engineering 11*, 445-463.

Hungr, O., Leroueil, S., & Picarelli, L. (2014). The Varnes classification of landslide types, an update. *Landslides 11*, 167-194.

Janbu, N. (1973). Slope Stability Computations. *Embankment - Dam Engineering: Casagrande Volume, John Wiley & Sons, Inc., New York* , 47-86.

Janbu, N., Bjerrum, L., & Kjaernsli, B. (1956). Veiledning ved losning av fundamenteringsoppgaver. *Norges Geotekniske Institutt Publikasjon Nr. 16*.

Kellogg, K. S., Shroba, R. S., Bryant, B., & Premo, W. R. (2008). Geologic Map of the Denver West 30'x60' Quadrangle, North-Central Colorado. *USGS*.

Koizumi, Y., Yokota, Y., Date, K., & Fujisawa, K. (2010). Numerical Analysis of Landslide Behavior Induced by Tunnel Excavation. *European Rock Mechanics Symposium (EUROCK 2010)*, 555-558.

Lee, F. T., & Mystkowski, W. (1979). Loveland Basin Slide, Colorado, U.S.A. *Developments in Geotechnical Engineering Vol. 14 Part B*, 473-514.

Lovering, T. S., & Goddard, E. N. (1950). Geology and Ore Deposits of the Front Range Colorado. *Geological Survey Professional Paper 223*.

Lu, N., Wayllace, A., & Oh, S. (2013). Infiltration-induced seasonally reactivated instability of a highway. *Engineering Geology 162*, 22-23.

MacRobert, C. (2018). Factors of safety and probabilities of failure in geotechnical engineering: What do we mean? *Civil Engineering*.

Matsuo, N. S., & Yamashita, S. (1968). Weathering of the Granite Soils annd its Influence on the Stability of Slopes. *Kyoto University, Fac. Engineering, Vol. 30, pt. 2*, 85-93.

Mattei, F. A. (1965). Engineering and Construction Report of Straight Creek Pilot Tunnel. *Tech. Rep. Denver, Colorado: Colorado Department of Highways*.

Miles, G. N., & Mattei, F. A. (1965). Final Geologic Report of the Straight Creek Pioneer Tunnel. *Tech. Rep. Denver, Colorado: Colorado Department of Highways*.

Morgenstern, N. R., & Price, V. E. (1965). The Analysis of the Stability of General Slip Surfaces. *Geotechnique, Vol. 15, No. 1*, 77-93.

Rehman, H., Wahid, A., Muntaqim Naji, A., Jung-joo, K., Rini Asnida, A., & Han-kyu, Y. (2018). Review of Rock-Mass Rating and Tunneling Quality. *Applied sciences, 8*, 1250.

Richards, D. B. (1963). Engineering Geology of the Proposed Straight Creek Tunnel, Clear Creek and Summit Counties, Colorado. *Colorado School of Mines Repository* .

Robinson, C. S., & Lee, F. T. (1964). Engineering Geology of Straight Creek Tunnel Site, Colorado. *Symposium on Soil Exploration, West Conshohocken, PA: ASTM International*, 17-28.

Robinson, C. S., & Lee, F. T. (1965). The Validity of Geologic Projection a Successful Example: The Straight Creek Tunnel Pilot Bore, Colorado. *U.S. Geological Survey*.

Robinson, C. S., & Lee, F. T. (1967). Results of Geologic Research at the Straight Creek Tunnel Pilot Bore, Colorado. *Committee on Engineering Geology, 46th Annual Meeting*.

Robinson, C. S., Lee, F. T., Moore, R. W., Carroll, R. D., Scott, J. H., Post, J. D., & Bohman, R. A. (1972). Geological, Geophysical, and Engineering Investigations of the Loveland Basin

Landslide, Clear Creek County, Colorado, 1963-65. *U.S. Geological Survey Professional Paper 673-A, B, C, D, E, F, G*.

Robinson, C. S., Lee, F. T., Scott, J. H., Carroll, R. D., Hurr, R. T., Richards, D. B., . . . Abel, J. F. (1974). Engineering Geologic, Geophysiscal, Hydrologic, and Rock-Mechanics Investigations of the Straight Creek Tunnel Site and Pilot Bore, Colorado. *USGS Professional Paper 815*.

Satici, Ö., & Ünver, B. (2015). Assessment of Tunnel Portal Stability at Jointed Rock Mass: A comparative Study. *Computer and Geotechnics, 64*, 72-82.

Spencer, E. (1967). A Method of Analysis of the Stability of Embankments Assuming Parallel Inter-Slice Forces. *Geotechnique, Vol 17*, 11-26.

Stead, D., & Wolter, A. (2015). A Critical Review of Rock Slope Failure Mechanisms: The Importance of Structural Geology. *Journal of Structural Geology* .

Taylor, D. W. (1948). *Fundamentals of Soil Mechanics.* New York: Wiley.

Terzaghi, K. (1962). Stability of Steep Slopes on Hard Unweathered Rock. *Geotechnique, Vol. 12*, 251-263.

U.S. Department of Transportation. (2009). Technical Manual for Design and Construction of Road Tunnels - Civil Elements. *Publication No. FHWA-NHI-10-034*.

USACE. (1970). Engineering and Design: Stability of Earth and Rock-Fill Dams. *Manual No. 1110-2-1902*.

USACE. (2003). Engineering and Design: Slope Stability. *Manual No. 1110-2-1902*.

USBR-USACE. (2015). *Best Practices in Dam and Levee Safety Risk Analysis.*

USGS. (1935). Geologic Map of the Montezuma Quadrangle, Colorado. *Professional Paper 178 Plate 3*.

USGS. (n.d.). *Earthquake Glossary*. Retrieved from https://usgs.gov: https://earthquake.usgs.gov/learn/glossary/?term=fault%20gouge

Varnes, D. (1954). Landslide types and processes. *Landslides and Engineering Practice* (pp. 20-47). Washington, DC: Highway research board. National Academy.

Vlachopoulos, N., & Vazaios, I. (2015). Case Study: The Influence of Tunnelling on Slope Stability. *GeoQuebec 2015 Conference*.

Wang, I. (2019). Safety Assesment of Tunnel Portals for Site Selection Based on Spatial Information Geoprocessing. *Infrastructures 2019, 4, 70* .

Wang, J., Zeng, Y., Xu, Y., & Feng, K. (2017). Analysis of the Influence of Tunnel Portal Section Construction on Slope Stability. *Geology, Ecology, and Landscapes*, 56-65.

Wayllace, A., Lu, N., & Godt, J. (2017). *In-situ monitoring of infiltration-induced instability of I-70 embankment west of the Eisenhower-Johnson memorial Tunnels, Phase II.* Report No. CDOT-2017-12.

Zhang, Z., Zhao, Q., Xu, C., & Xu, X. (2017). Interaction Analyses between Tunnel and Landslide in Mountain Area. *Journal of Mountain Science 14(6)*, 1124-1139.

APPENDIX A - DATA FROM THE PROJECT

Table A.1: Geomechanical properties of Silver Plume Granite, Idaho Spring Formation rocks, and fault gouge at the research site.

Material	γ $\left(\frac{\mathbf{MN}}{\mathbf{m^3}}\right)$	ν	MPa)	$\emptyset'$ deg)	MPa)	CS MPa)	SI_P	SI_R	i		
SPG	.02590	.3	5,000			79.6	5	6.3	3		.0105
ISF	.02600	.18	5,000	7.5	1.9						
Landslide	.02453	.3	00	4							.5
Buttress Fill	.02354	.3	00	0	.0689						.5

Note: γ is the unit weight, ν is the poisons ratio, E is Young's modulus, $\emptyset$ is the internal friction angle, c is the

Table A.1: Parameters used to perform sensitivity analyses of the slopes in the vicinity of the EJMT

Material	Parameter	Proposed Value	Range
ISF	$\emptyset'$ (degree)	37.5	24.4 – 45
	c' (MPa)	21.9	14.2 – 29.5
	Depth to GWT (ft)	-	0 – 85
	Snow Loads (MPa)	-	0 – 0.072
SPG	UCS (MPa)	179.6	89.8 – 179.6
	GSI_P	55	27.5 – 55

Note 1: The proposed values correspond to those reported in Table 2.2.

Note 2: $\emptyset'$ is the internal friction angle, c' is cohesion, GWT is groundwater table, UCS is the unconfined compressive strength, and GSI_P is the peak GSI.

Table A.2: Top six possible alignments for the new tunnel bore at the research site – Based on Alexander (2022)

West Portal	East Portal

Alignment No.	Latitude	Longitude	Elevation (ft)	Latitude	Longitude	Elevation (ft)	Length (mi)	Max Depth (ft)	Mean Depth (ft)	Fault Zone Occurrence (%)
211	39°40'33.12"N	105°56'4.82"W	11,342	39°40'26.86"N	105°54'21.82"W	11,338	1.50	1,290	584	29.9
243	39°40'11.52"N	105°56'41.39"W	11,434	39°40'26.69"N	105°54'17.38"W	11,325	2.07	1,273	646	44.0
2273	39°40'39.43"N	105°56'2.43"W	11,290	39°40'40.68"N	105°54'22.28"W	11,178	1.43	1,358	722	30.9
2929	39°40'11.50"N	105°56'41.12"W	11,431	39°40'41.38"N	105°53'25.42"W	11,127	2.84	1,375	499	48.3
4495	39°40'46.12"N	105°56'15.76"W	11,209	39°40'51.05"N	105°54'9.29"W	11,111	1.80	1,401	715	25.0
5448	39°40'49.85"N	105°55'58.21"W	11,302	39°40'58.11"N	105°54'5.23"W	11,337	1.62	1,171	656	0.0
8131	39°40'46.33"N	105°55'58.42"W	11,291	39°41'12.38"N	105°53'22.00"W	11,172	2.23	1,155	538	26.9

APPENDIX B – TECHNOLOGY TRANSFER ACTIVITIES

1 Accomplishments

1.1 What was done? What was learned?

We have developed a methodology to determine the potential impact of tunnel construction on the increased landslide susceptibility of an area that already has experienced significant ground movement. Both deterministic and probabilistic factor-of-safety calculations were used. The methodology was specifically applied to the future extension of the Eisenhower-Johnson Memorial Tunnel, where decisions must be made on determining the locations of additional tunnel bores that will increase the vehicular capacity of the existing tunnels. Some of the potential locations of the additional tunnel bores will pass through areas where some landslides have already occurred. There is concern that drilling tunnels beneath or close to the sensitive areas may re-trigger the old landslides. The minimum distance between a dual-bore tunnel and the face of the slope at which slope stability is virtually unaltered was analyzed using two-dimensional numerical simulations. The results from a deterministic and probabilistic analysis of approximately 600 simulations suggest that slope stability increases as tunnel bores are translated into areas of increasing overburden

1.2 How have the results been disseminated?

Dissemination through one international conference presentation. Furthermore, Simon Baeza-Faundez's MS thesis was funded by UTC-UTI and is archived at Colorado School of Mines Library. A copy of his report was provided to the Colorado Department of Transportation to help them decide on the locations of additional future tunnel bores to increase the vehicular capacity of the Eisenhower-Johnson Memorial Tunnel located on I-80.

2 Participants and Collaborating Organizations

Name: Colorado School of Mines
Location: Golden, CO, USA
Contribution: All research performed on campus

Name: Colorado Department of Transportation
Location: Golden, CO, USA
Contribution: Data on the Eisenhower-Jonhson Memorial Tunnel

3 Outputs

Conference Publication

Gutierrez, M. and Baeza-Faundez, S. (2023), **"**Effects of tunnel construction in landslide-prone areas," Proceedings, 6th World Landslide Forum, Florence, Italy, November 14-17, 2023.

4 Outcomes

The study showed that tunnel-slope interaction was minimized past a horizontal distance of 5.5 times the diameter of the tunnels into the slope.

5 Impacts

This research provides a general trend that could be applied to other projects with geomechanical properties and slope geometry within the ranges used in this study.